Low energy properties of identical and strongly correlated particles

Wolfgang Häusler

Angaben zur Veröffentlichung / Publication details:

Häusler, Wolfgang. 1996. "Low energy properties of identical and strongly correlated particles." *Annalen der Physik* 508 (5): 401–45. https://doi.org/10.1002/andp.2065080502.

Low energy properties of identical and strongly correlated particles

W. Häusler

I. Institut für Theoretische Physik, Jungiusstr. 9, D-20355 Hamburg, Germany

Abstract. Interesting qualitative consequences can arise from the quantum mechanical identity among strongly correlated particles that carry spin. This is demonstrated for properties connected with the low energy excitations in molecular and electronic systems. Spatial permutations among the identical particles are used as the key features.

The particular behaviour of rotational tunneling molecules or molecular parts under the influence of dissipation are discussed together with the consequences arising for conversion transitions. The relationship between the thermal shifting of the tunneling line and the conversion rate at low and at elevated temperatures is explicated. The valuable information, that can be extracted from the conversion behaviour after isotopical substitution, is explained in detail. At low temperatures qualitative changes are predicted for the conversion rate by deuteration. Weakly hindered rotors show, also experimentally, drastic isotopic effects.

The second part is devoted to finite systems of strongly interacting electrons that appear in semiconductor nano-structures. The lowest excitation energies are strongly influenced by the interaction. They can be understood and determined starting from the limit of crystallized electrons by introducing localized many particle 'pocket states'. The energy levels show multiplet structure, in agreement with numerical results. The total electron spin, associated with the low energy excitations, is crucially important for the nonlinear transport properties through quantum dots. It allows for instance to explain the appearance of negative differential conductances.

Keywords: Strong correlations; Tunneling; Spin excitations; Rotational tunneling; Nano-structures.

1 Introductory remarks

1.1 Motivation

The ability to describe interference and to attribute wave nature to particles is commonly considered as the prime feature of quantum mechanics. All tunneling phenomena are related to this aspect. These effects appear if the actions involved reach the order of Plank's constant $\hbar$. A second, in principle equally central aspect of quantum mechanics is to account in a rigorous way for the 'identity' among more than one particle. In contrast to the former property this latter aspect cannot be obtained by suitably generalizing classical mechanics for instance by allowing a certain parameter to take a nonzero value. This second feature of quantum mechanics has been detected historically later than the quantum numbers for single particles. Pauli postu-

lated the requirements to describe collections of same particles [1] in order to explain certain spectral multiplicities observed for electronic transitions in atoms.

The identity among spin carrying particles can lead to interesting physical consequences. This is shown in the present work for two particular examples. In the second chapter molecules or parts of molecules are investigated in which discrete rotations correspond to permutations of identical nuclei so that the Pauli principle imposes constraints upon the orientational wave functions and the nuclear spin. The most famous example is the dumbbell-like hydrogen molecule where the low temperature physics is entirely determined by the existence of two spin species, *'ortho'* and *'para'* H_2. Examples for other molecules showing qualitatively similar properties are the tetrahedrically symmetric methane CH_4, or the triangular $-CH_3$ group. Isotopic substitution of the identical protons by deuterons with approximatively twice the mass and spin $s = 1$, obeying Bose statistics, opens experimentally extremely conclusive insights to the physics of 'rotational tunneling' phenomena.

In the third chapter finite electron systems enclosed within very small artificial cavities fabricated on the basis of semiconductor hetero-structures are investigated. These *quantum dots* only contain microscopically small numbers $1 \lesssim N \lesssim 100$ of electrons. Contrary to the usual situation in atomic physics the Coulomb interaction causes strong correlations since the electron motion is restricted to two dimensions and the density is low. This yields not only the by now well known single electron (charging) effects in transport measurements due to the relatively large energies associated with changes in the number of electrons enclosed by the cavity but also considerably modified excitation properties. Both influences directly measurable quantities. Structures become visible in linear or nonlinear transport as well as in optical spectra. Instead of a homogeneous charge density distribution the electron system 'crystallizes'. This causes quantitative changes in the ground state energies and has even qualitative consequences for the excitation spectra compared to what is expected from (effectively) independent electrons. In these systems the low energy excitations can be traced back to rates for identical particles to interchange their equilibrium places, similar to the rotational tunneling systems. And, the total spin of a many electron wave function is again related to its energy via the Pauli principle. The approach presented here opens a unified description of the low energy properties in strongly correlated systems of identical nuclei or electrons.

1.2 Introduction

1.2.1 Equivalent versus Identical Particles

Already the Gibbs paradoxon demonstrates that indistinguishable particles cannot consistently be described by classical mechanics. On one hand side the entropy of two boxes containing N_1 and N_2 "equal" gas particles is independent of the wall between them only if the number of permutations $\binom{N_1+N_2}{N_1}$ is somewhat artificially divided out from the classical number of accessible states. On the other hand, classical mechanics allows to index each individual member of an ensemble of either equivalent or different particles since its trajectory can in principle be followed in phase space, the 'arena' of accessible classical states, with arbitrary accuracy (the difficulties which arise in nonlinear dynamics after long times do not weaken this argu-

ment). Particles may interchange their coordinates in phase space during the time evolution so that the restriction to its 'irreducible' part, as postulated in classical statistical mechanics, does not seem natural.

Quantum statistical mechanics solves this unpleasant point satisfactorily. The uncertainty principle undermines already the definition of a trajectory attached to a certain particle. Quantum particles cannot be identified by external properties like position or momentum. Particles are considered to be *"identical"* if they cannot be distinguished by any internal property (i.e. the discrete eigenvalue of an observable which should be a constant of motion). The symmetrization postulate restricts the 'arena' of accessible quantum states, the (product-) Hilbert space of N particles, to its symmetrized part[1]. Individual particles cannot be identified. Under the time evolution the system never leaves this part of the arena. This is essentially the postulate stated by Pauli [1] to treat identical particles, though the original formulation was slightly different. Its quantitative consequences are in agreement with all experimental observations. The treatment of *particle identity*, without any contradictions, is one of the central features of quantum mechanics.

The symmetrization refers to permutations among the indices attached by choice to the particles. The symmetry group S_N of the permutations of N elements [2] is therefore of importance. The only two one-dimensional irreducible representations of this group are realized in nature and correspond to Bosons (totally symmetric) and Fermions (totally antisymmetric), respectively. All higher dimensional representations do not correspond to any particle type.

The identity or non-identity of particles has quantitative consequences. An example is the potential scattering among equivalent particles. Assume them to be 'similar', without obvious differences e.g. concerning their masses, the differential scattering cross section between two particles

$$d\sigma = (|A(\theta)|^2 + |A(\pi - \theta)|^2)d\Omega$$

in the center of mass system is symmetric around forward scattering $\theta = \pi$, $A(\theta)$ being the scattering amplitude. Identity of the particles yields a qualitative enhancement around $\theta = \pi/2$

$$d\sigma = |A(\theta) + A(\pi - \theta)|^2 d\Omega$$

in comparison with the case of equivalent but not identical particles due to the 'exchange degeneracy'.

1.2.2 Rotational tunneling

The existence of the two species "ortho-" and "para-" hydrogen has already been mentioned. Similar systems will be the main subject in Chapter 2. After their discovery in 1929 [3] the two species were even believed to be chemically different in view of their considerable dissimilarity in various quantities like the electrical quad-

[1] In the present article "Symmetrization" includes, if applicable, "Antisymmetrization"

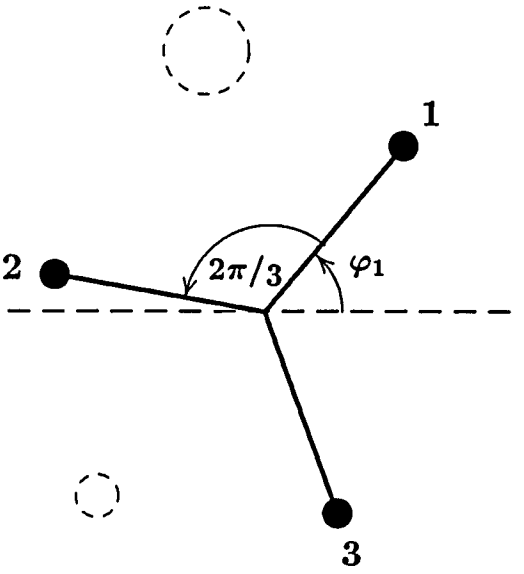

Fig. 1 Illustration of a methyl rotor CH_3 in an unsymmetric crystalline surrounding. The wave function must be invariant with respect to $2\pi/3$ rotations that correspond to an *even* permutation of the protons.

rupol moment, the nuclear magnetic susceptibility and, most seriously, in the ground state energy differing by 171 Kelvin. Later, however, the extremely slow "conversion" of the ortho-species into the para-species has been observed. The rate depends on temperature and pressure but no chemical reaction is involved. The enormous stability of rotational tunneling systems relies on the classically non existing quantity 'spin' in combination with the Pauli principle.

The term *"rotational tunneling"* is more commonly used [4] in the context of molecules with larger moments of inertia J than the one of H_2 with its extremely short bonding length. Our prominent example will be the methyl group CH_3 with a rotational constant of $B \approx 7$ Kelvin ($B_{H_2} \approx 85$ Kelvin). $B \equiv \frac{\hbar^2}{2J}$ establishes the energy scale for quantum effects to be important in the isolated rotor if intra-molecular vibrations are high in energy and can be ignored. In the surrounding of a solid each of these molecules can be oriented in different ways which are energetically precisely equivalent. This is their characteristic property. Transitions between the different equilibrium orientations are enabled by quantum mechanical tunneling. The corresponding discrete rotations permute identical particles (i.e. hydrogen nuclei in the aforementioned examples). Therefore the Pauli principle relates the transformation behaviour of the rotational eigenfunctions with the total nuclear spin.

In the example of H_2 the lowest eigenvalue is connected with a spatial wave function which is invariant with respect to rotations of the dumbbell by 180°. Identical particles, like protons, must carry spin to make this energy physically accessible. The total nuclear spin values $S = 0$ or $S = 1$ for the para- or the ortho-species explain e.g. their different magnetic susceptibilities. A dumbbell molecule composed of identical spinless particles (Bosons) cannot show eigenvalues associated with odd parities, and accordingly, the ground state of (hypothetical) spinless Fermions would have the energy $\hbar^2/J$. Spin carrying particles show richer energy spectra than spinless particles.

This statement can be generalized to the eigenfunction

$$\psi(x_1\sigma_1, \ldots, x_i\sigma_i, \ldots, x_j\sigma_j, \ldots, x_N\sigma_N) \tag{1.1}$$

of an N-particle Hamiltonian that is assumed to depend only on spatial coordinates. Then ψ remains invariant with respect to a permutation of the particle enumeration

$$\psi(x_1\sigma_1, \ldots, x_j\sigma_j, \ldots, x_i\sigma_i, \ldots, x_N\sigma_N) \tag{1.2}$$

(Bosons) or acquires a sign $(-1)^P$ (Fermions) proportional to the parity of the permutation P. On the other hand, ψ must have well defined transformation properties also with respect to permutations only among the coordinates $\{x_i\}$

$$\psi(x_1\sigma_1, \ldots, x_j\sigma_i, \ldots, x_i\sigma_j, \ldots, x_N\sigma_N) \tag{1.3}$$

or only among the spins $\{\sigma_i\}$ since these operations leave the Hamiltonian equally well invariant. Subsequent permutation of the spins in (1.3) finally must yield (1.2). Spin makes the not symmetrized, spatial part of the N-particle Hilbert space physically accessible. This increases the number of realized eigenvalues of the Hamiltonian (the energies are solely determined from spatial space).

Other operators acting on the N-particle system that depend only upon spatial coordinates, like phonon operators, must leave the transformation property (*symmetry*) of each eigenfunction unchanged with respect to the operations (1.3). This is the physical origin for the extraordinary thermal stability of the different rotational symmetry species. The energy scale on which temperatures influence the tunneling line observed in inelastic neutron scattering exceeds the energy difference Δ of the lowest rotational states (tunneling energy) by several orders of magnitudes. The Δ are typically in the μeV range while the corresponding lines shift and broaden only above temperatures of 20 or 30 Kelvin. This behaviour is completely different from what is observed for the tunneling of a single particle, that tunnels between e.g. two crystallographically equivalent sites by translational motion. In this latter case the quantum tunneling is observed to disappear at temperatures above Δ [5]. The inelastic peaks centered around $\pm\Delta$ on the energy axis merge with the broadened quasi-elastic peak. The dissipative influence of a phonon bath will be discussed in Section 2.1.

Conversion transitions between the states of different symmetries must involve operators acting simultaneously on spatial and on spin space [6]. An example is the neutron scattering operator which explains the direct observability of rotational tunneling by means of inelastic neutron scattering. Transitions associated with thermalization of the sample, e.g. between ortho- and para-hydrogen, require to change the symmetry of the rotational states. The observed times exceed the inverse tunneling frequencies typically by 6–15 orders of magnitudes (for many systems the value is not known and the experimental boundaries depend often on the patience of the experimentalist). The conversion transition, particularly its dependence on phonons, will be discussed in Section 2.2 where also the most important experimental techniques to measure these times are described.

1.2.3 Correlated electrons

The rotational tunneling excitations can be interpreted as being connected with processes of identical particles exchanging their equilibrium places. The use of localized

rotor states (*"pocket states"*) provides a conceptually very clear and successful starting point for a quantitative description of the spectra [7]. In the third chapter this approach will be generalized to finite systems of strongly interacting electrons as they appear in small semiconducting nano-structures. The many body wave functions have the same properties (1.1–1.3) as discussed before for nuclear coordinates and the low energy excitations can be related to processes where electrons interchange places in a similar way, cf. Section 3.2. The discrete energy levels are again intimately connected with total spin. The experimental probes are linear and nonlinear transport measurements. The set up is sketched in Fig. 2.

The many-electron levels in quantum dots are observed most successfully by nonlinear transport. Excitation energies can be observed within the difference $\mu_L - \mu_R$ of chemical potentials applied across the dot. Meanwhile this kind of experiments have been carried out at the Technische Universiteit in Delft, at the MIT in Cambridge, Mass., at the MPI in Stuttgart and at the UCBE in Berkeley. Apart from the structures which reflect the excitations energies in the current-voltage characteristic regions of *negative differential conductances* have been detected. The latter cannot be understood within traditional approaches. The consideration of the electron spin to build up the N-electron states in presence of strong interactions provides up to now the only explanation for this observation. In analogy to the Coulomb blockade this phenomenon has been called *"Spin Blockade"* [8].

More recently these selection rules are investigated more in detail. The transition rates [9] appearing in the master equation description of nonlinear transport [10] are influenced by the correlations in the electron states. Matrix elements of the qualitative type $\langle \psi^{(N+1)} | c^+ | \psi^{(N)} \rangle$ between an $(N+1)$- and an N-electron eigenstate play a role due to the electron passages through either of the barriers. The resulting currents have been calculated in [10, 11]. Only the detailed knowledge of these overlaps allows to extract energies and even interesting properties of the N-electron wave functions from experimental 'nonlinear transport spectroscopy'. Knowledge of the many electron states and energies are the basis for the understanding of excitation- and transport behaviours of semiconductor micro-structures.

The conductance at small applied voltages and low temperatures reveals the ground state properties of the electron system. The energies associated with addition or removal of single charges to or from the island can exceed the thermal energy if the island is sufficiently small. This is the origin of the single electron effects [12, 13] which have attracted considerable interest since their discovery. Low transmittivities $\frac{h}{e^2}/R_T \ll 1$ of the contacts to the electron reservoirs are necessary to suppress fluctuations of the number N of conducting electrons inside the island. Then N can be considered as a classical variable. The electron number on the island favoured by electrostatics is stable against small transport voltages so that the current vanishes. This phenomenon has been called "Coulomb blockade" [14]. Suitable choice of the island potential via the gate voltage V_G allows to establish degeneracy between the energies of the charge states N and $(N+1)$

$$E(N+1) = E(N) = \frac{(Ne)^2}{2C} - eV_G N \quad . \tag{4}$$

Then the current is finite. The periodic changes between finite and vanishing transport as a function of V_G (Coulomb blockade oscillations) have meanwhile been ob-

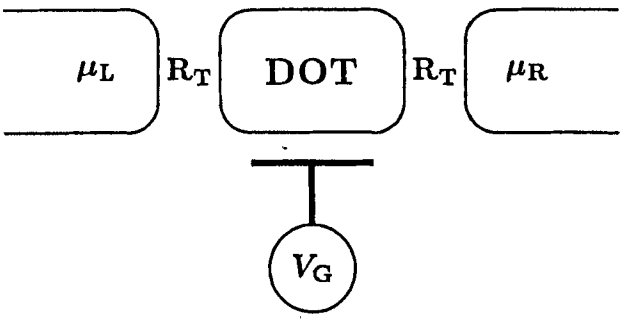

Fig. 2 Sketch of a transport experiment through a quantum dot. The transport voltage, given as the difference between the applied chemical potentials $(\mu_L - \mu_R)/e$, may be infinitesimally small or finite. The tunnel resistances R_T should be large compared to h/e^2 to suppress fluctuations of the electron number on the dot. The external gate voltage V_G allows to regulate the mean number of electrons on the island.

served by numerous experimental groups [15]. Each peak corresponds to a certain N in (4). The period is constant if the capacitance C is independent of N. This assumption is usually justified within a (simplified) mean field argument which is the basis of the "charging model" [12]. In presence of strong correlations this question is discussed in Section 3.1.1.

The Coulomb blockade has been observed in metallic [16–19] as well as in semiconducting islands [20–22]. The latter are called *"quantum dots"* [23]. Apart from easier possibilities to manipulate parts of the nano-structure, e.g. the heights of tunneling barriers, by gates quantum dots differ from the metallic counterparts in important physical properties since the Fermi-wave length is comparable to the diameter of the dot. This increases the level separation and facilitates the experimental observability of discrete excitation energies. Furthermore, the absolute number of conducting electrons is reduced to values $N < 10^2$ which is small compared to $N \sim 10^8$ found in metallic islands. Results calculated for finite systems need not necessarily be extrapolated to the macroscopic limit. The importance of the long range Coulomb interaction is, however, considerably increased on the scale of the Fermi energy due to the low electron density. Together with the reduced dimensionality for the electron motion to $d = 2$ in hetero-structures correlations are substantially enhanced compared to metals (electrons can avoid one another less easily than in $d = 3$). Exact energies and correlation functions have been compared with results obtained within selfconsistent Hartree Fock approximations [24, 25]. The mean field approximation turns out to be unreliable. Few electron systems in semiconducting hetero-structures have been called 'artificial atoms' [26] in analogy with the Mendelejev table of real atoms. However, unlike to situations in three dimensions or small mean electron distances, on the scale of the Bohr radius, effective single electron states (orbitals) cannot be defined for quantum dots. To describe ground- or even excitation-energies in the latter requires to take the correlations into account.

Since the work by Wigner [27] it is known that the long range Coulomb interaction leads to inhomogeneous 'crystallized' density-density correlation functions in the limit of a very large mean inter-particle distance $r_s \to \infty$. At short distances the inhomogeneity in the ground state shows up even in one dimension [28, 29]. The tendency of the kinetic energy to delocalise the particles decays $\sim r_s^{-2}$ and therefore

cannot compensate for the gain in potential energy connected with the crystallization. The boundary prevents continuous sliding of the finite crystal as a whole and establishes fixed particle positions. At large r_s these sites correspond to the minima of the electrostatic energy.

The localized electrons make immediately two types of excitation modes plausible. The first are vibrations of the electrons around their equilibrium positions due to the Coulomb forces between them. The corresponding phonon-like energies Ω can easily be shown to scale like $\Omega \sim r_s^{-3/2}$ by linearizing the interaction. A particle spin s leads to $(2s+1)^N$-fold degeneracy of each phonon level. Secondly, the electrons might exchange their positions by tunneling through the Coulomb barrier. Such interchanges must be included into the quantum mechanical eigen functions in order to avoid the enumerability of the electrons according to place numbers. These processes cause splittings of the phonon-like energy levels and give rise to the excitations of lowest energies. They are closely related to spin. The pocket state description introduced in Section 3.2 allows to calculate this low energy spectrum. In Section 3.4 the pocket state approximation is compared with results obtained by numerical diagonalisations.

The processes of electrons interchanging places should not be confused with the exchange integrals arising in the theory of Ferro-magnetism. The processes considered here tend to favour antiferromagnetic coupling between electron spins and therefore rather resemble the 'superexchange' discussed in the context of Hubbard models [30, 31]. The possible mapping of the continuous model for a quantum dot to suitably chosen spin-charge lattice models, keeping the correct low energy behaviour, is the subject of present research [32].

Localized many particle pocket states have been applied recently also to the problem of the magnetization of small rings threaded by a magnetic flux. It is common belief that the unexpectedly large values observed experimentally for the persistent equilibrium currents can only be understood by accounting for the electron-electron interaction. At least in presence of strong interactions the spin turns out to be an important ingredient to the behaviour of the current. A short summary of recent results has appeared in [33].

2 Rotational tunneling systems

2.1 Damping

In classical mechanics 'dissipation' can be described on a microscopic level as the consequence of frequent collisions with light particles [34]. The Langevin equation for the Brownian motion of a heavy particle contains random forces and a damping which is due to the back-reaction of the surrounding particles on the motion of the particle. It is related to the stochastic properties of the collisional forces through the fluctuation-dissipation theorem. Random forces without temporal correlations (white noise) lead to the friction $\sim \eta\dot{x}$ proportional to the instantaneous velocity of the particle.

This description of dissipation is based on a stochastic equation of motion for the coordinate $x(t)$ and cannot be quantized canonically. Attempts to formulate quantum dissipation, e.g. using explicit time-dependent Hamiltonians [35], describe either no true dissipation or violate basic principles of quantum mechanics. The formulation of 'friction' turned out to be a conceptual problem in quantum mechanics [36].

The most convincing pathway is provided by the theory of open quantum systems where the Hamiltonian

$$H = H_s + H_{ph} + H_I \tag{2.1}$$

includes a large number of external degrees of freedom described by H_{ph} to which the system of interest, H_s, is coupled through H_I. These theories have been developed [37–39] for the example of a harmonic oscillator coupled to an ensemble of reservoir oscillators. The Hamiltonian for the composed *system-plus-environment* can be quantized canonically. The dissipative influence shows up in the dynamics for the reduced density matrix describing the system.

Since the seminal work of Caldeira and Leggett [40] it became clear that the class of models (2.1) allows to describe the dissipative influence on typical quantum motions like tunneling. For calculational purposes the 'reservoir' of environmental degrees of freedom is preferably chosen as an ensemble of harmonic oscillators $H_{ph} = \sum_k \omega_k b_k^+ b_k$ that are coupled via H_I to the system, linearly in the Bose operators. The index k reminds of the quasi-momenta of quasi-particle excitations but translational invariance is actually not required. The treatment of the environment like harmonic oscillators can be motivated (though not rigorously proven) if the external coordinates are only weakly influenced by the system. This is the case in the limit of large numbers of environmental degrees of freedom if the coupling does not prefer a finite subset of the modes. The complete influence of H_I onto the system is contained in the 'coupled density of phonon states'

$$J(\omega) := \frac{\pi}{2} \sum_{k=1}^{n} \frac{g_k^2}{\omega_k} \delta(\omega - \omega_k) \quad , \tag{2.2}$$

where the strength g_k of the coupling to the k-th mode must be weak $g_k \propto n^{-1/2}$ in order to leave the energy for the system finite. The system of interest itself, however, can be influenced strongly by H_I so that a perturbational approach may be not valid. $J(\omega)$ is regarded as continuous for $0 \leq \omega \leq \omega_c$ up to the highest frequencies ω_c appearing in H_{ph}. For tunneling systems the low frequency part of $J(\omega)$ is most relevant.

The major advantage of the path integral representation of quantum mechanics [41, 42] is the possibility to integrate out the linear environment in (2.1) exactly [43]. The full quantum mechanical influence of the environment on thermostatic or dynamic quantities of the system can be cast into a functional [44] that depends only on the degrees of freedom of the system. The status of this approach in the context of quantum dissipative systems is most comprehensively, reviewed in the recent book of Weiss [45]. Among the prominent physical systems, where decisive theoretical results have been obtained, is the damped tunneling of hydrogen atoms between two equivalent crystalline sites in the presence of conduction electrons, the influence of the electrical impedance on the macroscopic quantum coherence in SQUIDS, and small islands showing Coulomb blockade. The dissipative environment determines the low temperature properties of a tunneling coordinate. The first system is most relevant to the present section.

Different temperature regimes have been found [46–50]. At high temperatures the scattering function

$$S(\omega) = \frac{1}{2\pi} \int \mathrm{d}t \, \mathrm{e}^{i\omega t} \langle x(0)\, x(t) \rangle \quad , \tag{2.3}$$

which is the temporal Fourier transform of the autocorrelation function [51] for the hydrogen position, can be explained already within classical statistical mechanics by thermally activated, random jumps over the potential barrier. The rates obey an Arrhenius law due to the Boltzmann probability distribution for the particle energy [52]. The autocorrelation function $\langle x(0)\, x(t) \rangle$ decays exponentially in time leading to a peak in the scattering function which is centered around $\omega = 0$ of Lorentzian shape (quasi-elastic peak). At reduced temperatures incoherent quantum tunneling adds to the classical particle transfer. Still the process can be described by a (Pauli-) rate equation for the occupation probabilities of the sites with its exponentially decaying solution. With further decreasing temperatures coherencies start to contribute at times even longer than the inverse tunneling rate. Thermal phase-breaking effects are diminished and the wave functions for the two hydrogen positions interfere constructively. For the case of hydrogen in Nb this first shows up as a broadening of the quasi-elastic peak according to the Kondo law $\sim T^{2K-1}$ for small Kondo parameters K (weak coupling) [53]. This type of broadening of the quasi-elastic peak is connected with the ohmic dissipation $J(\omega) \sim \omega$ for $\omega \ll \omega_c$ caused by conduction electrons; it would presumably not appear for damping by acoustical phonons. At temperatures of the order of Δ two tunneling peaks centered around $\omega = \pm\Delta$ start to appear (see Fig. 3). They reflect coherent oscillations of the hydrogen atoms between the two positions. Their intensity obeys detailed balance. The width of these inelastic tunneling peaks remains finite even at the lowest temperatures. This is a manifestation of the finite dissipative influence of a quantum mechanical environment at zero temperatures [40], in qualitative contrast to the classical friction described by a Langevin equation. Δ is the tunneling rate which itself may be renormalized by the phonons compared to the 'undressed' static value Δ_0. The experimental verifications, also concerning the other physical systems quoted above, have been extremely convincing [5, 18, 54–56].

Unfortunately, a satisfying solution of the rotational tunneling problem by means of the path integrals has up to now only been successful in the absence of dissipation. In [58] the rotor is treated as a harmonic oscillator which ignores the inherent non-linearity of a rotational tunneling system.

The popular example of a methyl group CH_3 can be described by one rotational coordinate φ if the rotor is taken as a rigid object and ignoring internal molecular modes of high energy [59]. The angles φ_i of the proton positions in polar coordinates define $\varphi \equiv (\varphi_1 + \varphi_2 + \varphi_3)/3$. The orientational Hamiltonian for a single molecule then reads

$$H_r = -B\partial_\varphi^2 + V \cos 3\varphi \quad . \tag{2.4}$$

Its invariance with respect to the unitary transformation $\varphi \longrightarrow \varphi + 2\pi/3$ follows from the identity of the protons and is, as the outstanding property of rotational tunneling systems, not affected through a coupling to phonons. The eigenfunctions ψ_Γ of

$$H = H_r + H_{ph} + H_I \tag{2.5}$$

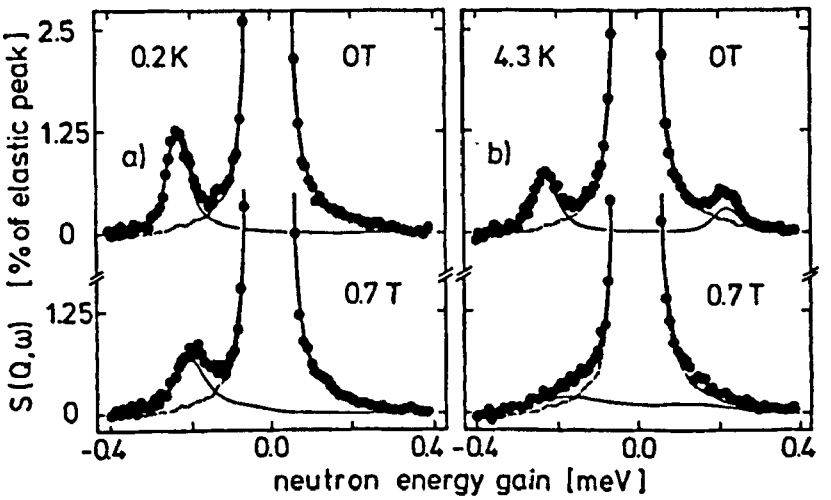

Fig. 3 Inelastic scattering function of hydrogen tunneling between two crystallographically equivalent sites in Nb, after [57]. The dissipation in this system is caused by conduction electrons that cannot be excited in the superconducting state (upper spectra). At finite magnetic fields superconductivity is suppressed and the dissipation broadens the tunneling peak even at low temperatures (left spectra). The two temperatures shown (0.2 and 4.3 Kelvin) give only a rough idea about the thermal broadenings and shifts of the tunneling lines. The elaborate analysis can be found in [5, 54] together with other details about this system.

transform according to the irreducible representations $\Gamma = A, E^a, E^b$ of the symmetry group C_3 with respect to $\psi_\Gamma(\varphi + 2\pi/3, \{x_k\}) = e^{i\kappa 2\pi/3}\psi_\Gamma(\varphi, \{x_k\})$ rotations, where

Γ	κ	$S\,(s=1/2)$	$S\,(s=1)$
A	0	3/2	0, 1, 3
E^a	+1	1/2	1, 2
E^b	−1	1/2	1, 2

(2.6)

and $\{x_k\}$ denote environmental coordinates. The Hamiltonian (2.5) cannot induce transitions between states of different symmetries, all matrix elements $H_{\Gamma\Gamma'}$ vanish for $\Gamma \neq \Gamma'$. E-symmetric eigenfunctions of (2.5) can exist in nature only if the (nuclear) spin of the identical particles is nonzero. Substitution of the protons by other Fermions or Bosons of finite spin does not alter the set of observable eigenvalues obtained from (2.4), only the rotational constant B may change. The different total spins S, obtained from the Pauli principle for $s = 1/2$ or $s = 1$ particles, are listed in (2.6). Spinless identical particles show only the eigenvalues connected with $\Gamma = A$. The difference between the ground state (A-symmetric) and the lowest eigenvalue associated with an E-symmetric eigenfunction defines the tunneling splitting Δ at zero temperature (cf. Fig. 5, ψ_{E^a} and ψ_{E^b} form a Kramers doublet [60] and are energetically degenerated).

For the isolated rotor (2.4) Δ can be estimated as a function of the barrier height V using the instanton method of Coleman [61, 62]. One has to take care of the fundamental difference between a quantum mechanical angle coordinate with possible eigenvalues $\varphi \in [0, 2\pi[$ and a classical angle, appearing in the path integral, that can take all real values $\varphi(t) \in]-\infty, +\infty[$. Classically, the winding number of the rotor

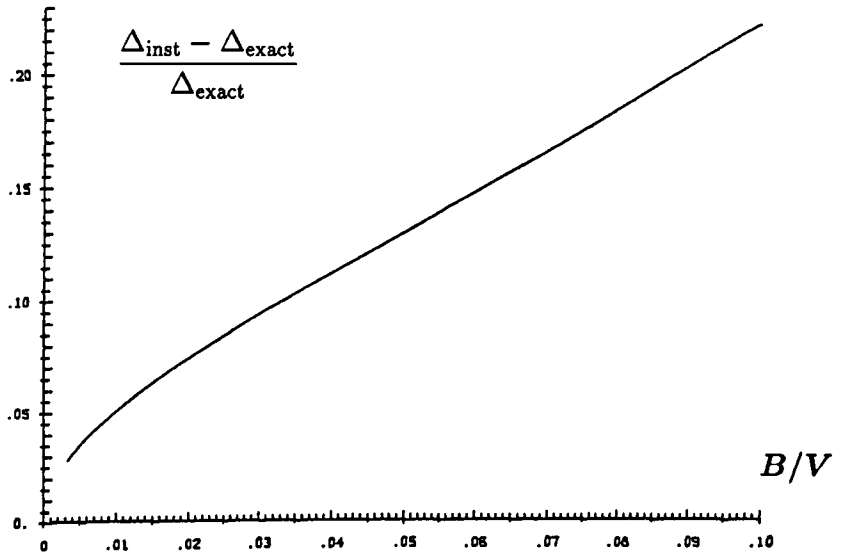

Fig. 4 Difference between the exact tunneling energy Δ_{exact} associated with the Mathieu potential (2.4) of amplitude V/B and the tunneling energy within instanton approximation Δ_{inst} (2.7) on the scale of Δ_{exact}. In the shown range of parameters the value for Δ itself varies by 7 orders of magnitudes.

can be counted by observing the system. This difference shows up in the requirement to decompose the paths according to winding numbers [63]. The resulting formula [64] to estimate the tunneling splitting of (2.4)

$$\frac{\Delta_{inst}}{B} = 12\sqrt{\frac{3}{2\pi}}\left(\frac{2V}{B}\right)^{3/4} e^{-\frac{4}{3}\sqrt{2V/B}} \tag{2.7}$$

within 'dilute instanton-gas approximation' reproduces extremely well numerically obtained values for Δ, cf. Fig. 4, and agrees with the formula found previously by empirical fits [65].

The tunneling splitting Δ can be viewed (rather for pedagogical than for true calculational purposes, cf. [66]) as the overlap integral between harmonic oscillator wave functions centered around adjacent minima of the potential e.g. $\varphi \approx 0$ and $\varphi \approx 2\pi/3$. Higher excited levels of (2.4) are approximatively given as harmonic excitations ("librations") in the potential minima with energy $\Omega \approx \sqrt{18\,VB}$.

Rotational tunneling systems are ideal to study the quantum dissipative influence caused by the coupling to the crystalline lattice because the tunneling is observable e.g. by inelastic neutron scattering [67–69] or by high field NMR [70] up to temperatures exceeding Δ by many orders of magnitudes.

A typical series of spectra are shown in Fig. 6. Note that the magnitudes of T/Δ differ considerably from those shown in Fig. 3. At low temperatures sharp tunneling peaks centered around $\omega = \pm\Delta$ are visible on either side of the energy scale. With rising temperature their position shifts and they broaden until they merge under the broadened quasi-elastic peak. This happens at temperatures which are much higher than in translational tunneling systems.

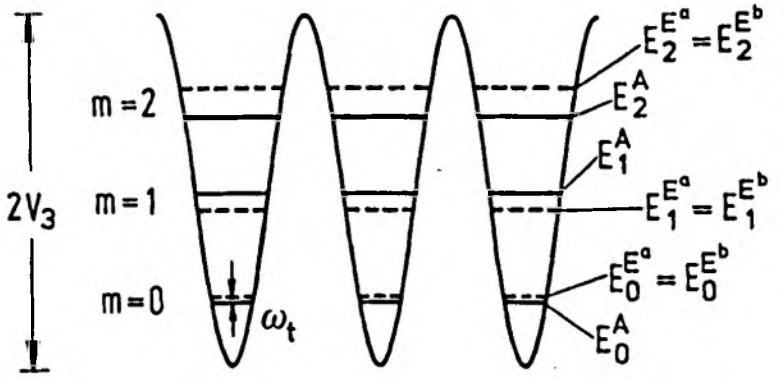

Fig. 5 Energy level scheme of (2.4) describing a CH_3 rotor. Typical values for $\omega_t \equiv \Delta$ are few μeV while the librational energy $E_1^\Gamma - E_0^\Gamma \equiv \Omega^\Gamma$ is typically 10 meV. The spatial parts of the wave function are of different symmetry ($\Gamma = A, E^a, E^b$). Totally symmetric states with respect to even proton permutations (i.e. $2\pi/3$ rotations) are achieved through the spin space.

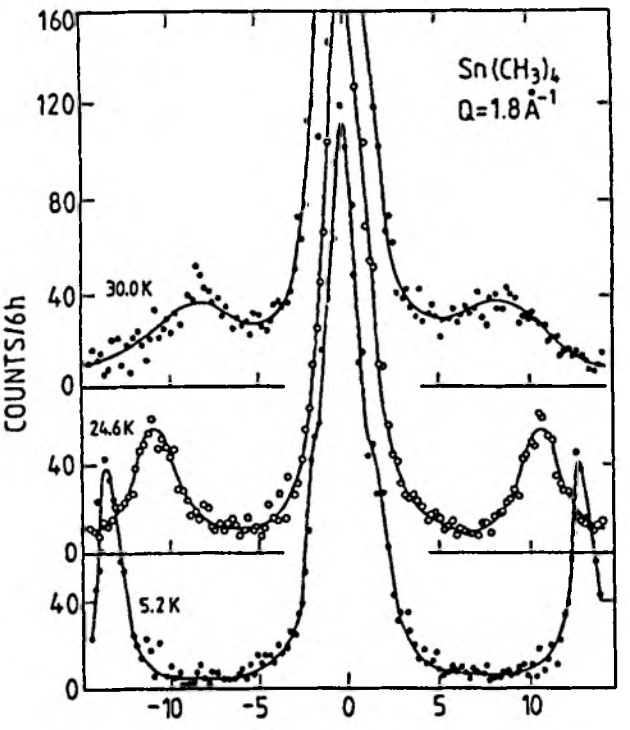

Fig. 6 High resolution inelastic neutron scattering spectra from $Sn(CH_3)_4$ for temperatures up to 30 Kelvin, after [71].

The scattering function [72] for a one dimensional rotor (2.4) at momentum transfers small compared to its inverse radius can be written as [64]

$$S(\omega) = \int \mathrm{d}t\, \mathrm{e}^{i\omega t} \langle \mathrm{e}^{-i\varphi(0)} \mathrm{e}^{i\varphi(t)} \rangle \tag{2.8}$$

where the full Hamiltonian (2.5) determines the Heisenberg operator $\varphi(t)$ and the thermal quantum average $\langle \ldots \rangle$. A variety of attempts have been made to describe the

temperature dependence of $S(\omega)$ for a rotational tunneling system theoretically. The phenomenological assumption of random transitions between the librational rotor levels of given symmetry Γ (cf. Fig. 5), in the spirit of [73], can explain an exponential shifting and broadening of the tunneling line with temperature [74]. Quantitative agreement with experiments is, however, often poor. The T^4-law for the shift has been obtained in perturbation theory first by Hüller [66]. Later it has been refined to extract also broadenings from complex self energies [64, 75, 76]. The numerical study of the coupling to one oscillator mode allows to check the regime of validity for the perturbation theory – the experimental situations were estimated to be in many cases beyond this regime [64].

More recent attempts to extend the range of coupling strengths are based on simulations where stochastic forces act on an intermediate classical particle [77, 78], and on substituting the rotor by a harmonic oscillator and a spin [79]. The two possible values of the latter simulate the two sets of eigenenergies related to the symmetries A or E so that the combined system reproduces the lowest 4 levels of the spectrum shown in Fig. 5. This description enables, in principle, to allow for strong rotor-phonon couplings. Apart from the T^4-law for the shift, interestingly, it predicts a non–Arrhenius like T^7-behaviour for the thermal broadening of the tunneling line [80]. Another recent approach is based on approximations to the time-dependent reduced density matrix for the rotor and allows to separate coherent from incoherent transitions between its matrix elements due to environmental fluctuations [81]. Even an ohmic dissipation $J(\omega) \sim \omega$ for $\omega \ll \omega_c$, which has been assumed, though not present in real systems, does not yield incoherent tunneling transitions.

Table 1 compares the known temperature dependencies of the scattering function for rotational and translational tunneling systems. The CH_3 group and the spin-Bose system are considered as representatives. In both cases a coupling to acoustical phonons is considered which in absence of particular crystallographic symmetries is described by

$$J(\omega) \sim \begin{cases} \omega^3 & \text{for } \omega \ll \omega_c \\ 0 & \omega > \omega_c \end{cases} . \tag{2.9}$$

The comparison should be appreciated with some caution because different types of approximations are used. The perturbational results for the rotational tunneling systems are valid only at weak damping *and* low temperatures. The increased effective influence of the environment on the rotor with temperature undermines the perturbational description. The high temperature behaviour, where $S(\omega)$ consists of a quasielastic peak that broadens according to $\sim e^{-2V/T}$ and that can well be explained by classical hopping [4], cannot be recovered within perturbation theory – a closed theory valid for the entire range of temperatures is still lacking.

The most general results for the spin-Boson system were obtained within the noninteracting bounce approximation (NIBA) where retarding effects owing to the phonon bath, calculated first by Feynman and Vernon [44], were taken into account only between adjacent transitions of the spin [48]. For dissipation of the type (2.9) this is believed to be reliable for all temperatures and coupling strengths [45, 47, 48]. The non-perturbative results make the spin-Boson model to *the* best understood quantum dissipative system [45, 48, 83, 84]. When the temperatures approach the energies of the vibrations of hydrogen atoms within one of the crystallographic potential minima

Table 1 Comparison of the thermal developments of $S(\omega)$ of translational and rotational tunneling systems. A low frequency behaviour of the environment $J(\omega) \sim \omega^3$ is assumed. The results for the spin-Boson model are obtained within the NIBA [53, 82] while results for the CH_3 rotor rely on perturbation theory [64, 75, 76]. The spin-Boson system does not show a quasi-elastic peak; for a double well system an Arrhenius behaviour with an activation energy given by the barrier height, similar to the rotational tunneling system, would be expected.

	Translational tunneling of Spin-Boson model	Rotational tunneling of CH_3 rotor
Broadening of tunneling line	$\sim$ const$+e^{-\Delta/T}$	$\sim e^{-\Omega/T}$
Width of quasi-elastic line	–	$\sim e^{-2V/T}$
Low temperature shift of tunneling line	$\sim +T^4$	$\sim \mp T^4$ for $\left\{\begin{smallmatrix}\text{shaking}\\ \text{breathing}\end{smallmatrix}\right\}$ phonons

its dynamics can no longer be reduced to a spin and the two-state model becomes inapplicable. In this case a continuous double minimum potential has to be used that yields immediately the correct high temperature limit in path integral representation by either looking at the rate for tunneling escape out of one of the minima [46] or at the incoherent tunneling in a double well [85].

The low temperature broadenings of the tunneling lines in both cases of Table 1 are of Arrhenius type but with considerably different 'activation energies'. This reflects the very different mechanisms that cause the two correlation functions (2.3) and (2.8) to decay through the damping caused by the environment. Low energy phonons with $\omega_k \approx \Delta$ stimulate most effectively transitions between translational tunneling states while they cannot induce direct transitions between states of different symmetries in rotational tunneling systems. In the latter case the lowest symmetry conserving excitations are of energy $\Omega^\Gamma \equiv E_1^\Gamma - E_0^\Gamma$ where E_i^Γ denotes eigenvalues to (2.4), cf. Fig. 5. Unfortunately only very poor knowledge exists about the rotor-phonon coupling $J(\omega)$ in molecular crystals containing rotational tunneling groups. The first serious and very elaborate attempt to extract this information from the measured phonon density of states has been carried out only recently [86]. The interatomic potentials had to be adjusted compared to literature values to explain the observed temperature dependence of the tunneling line when supposing lowest order perturbation theory for broadening and shifting.

Even in next order of perturbation theory phonons of frequency $\omega_k \approx \Omega$ turn out to be most important [64]. The two phonon contributions can, however, explain slight differences observed in the activation energies $\mathcal{E}^E > \mathcal{E}^A$ [69] as a density of states effect. This is unexpected within one phonon contributions because $\Omega^E < \Omega^A$ even for more general single rotor potentials than in (2.4). Also the residual width of the tunneling line at zero temperature can be estimated within fourth order perturbation theory. It is proportional to $J(|\delta\Delta|)$ where $\delta\Delta$ is the renormalization of the tunneling frequency due to the dissipation at zero temperature and therefore in agreement with all experimental observations, and in contrast to translational tunneling systems (Fig. 3), extremely small (cf. (2.9)).

The low temperature shift of the tunneling line is given as an integral over $J(\omega)$ which yields the T^4 dependence in the presence of Debye phonons. Similar to the dissipative quantum escape thermal fluctuations enhance the translational tunneling rate [45, 48] which corresponds to a positive shift. On the other hand, the majority

of rotational tunneling systems show negative shifts with temperature. Within Allen's phenomenological theory, assuming random symmetry conserving transitions between rotor states [74] the negative shift is explained by thermal admixtures of the negative tunneling frequency in the librationally excited states to the ground state tunneling frequency (i.e. by $\Omega^E < \Omega^A$). Also the first perturbation theories considering the coupling to a phonon bath [66, 75] have been simplifying the rotational degree of freedom too far so that the origin for positive contributions to the shift remained hidden. The first clear experimental observation of a positive shift at low temperatures [68, 87] has given credit to the results which had been obtained first from the numerically exact coupling to one oscillator mode [64]. The sign of the shift has been related to the type of the rotor-phonon coupling. Modes that modulate the phase of the orientational potential $\sim g_k \sin 3\varphi(b_k + b_k^+)$ of the rotor (shaking modes), cause a decreasing tunneling splitting with temperature while modes that modulate the amplitude of the tunneling barrier $\sim g_k \cos 3\varphi(b_k + b_k^+)$ (breathing modes) lead to thermal enhancement of the tunneling splitting. Within lowest order perturbation theory only the shaking modes cause the exponential line broadening with the activation energy of order Ω as it is frequently observed. Two phonon processes, however, make also breathing type phonons to contribute to the line broadening. These two different kinds of modes are extremely important to understand the behaviour of conversion rates as they are discussed in the subsequent Section.

2.2 Symmetry species conversion

It is the characteristic feature of rotational tunneling systems that symmetry changing transitions occur extremely slowly compared to the inverse frequencies of environmental or tunneling modes. Molecular hydrogen has already been mentioned. The weakness of the transition operators, see below, is only one reason for this extreme stability. In order to take place at low temperatures the conversion transition needs low energy fluctuations which are provided only rarely by the surrounding even if the coupling to the tunneling system is strong.

At temperatures of the order of the tunneling splitting Δ the thermal equilibrium of molecular crystals can easily be disturbed by sudden jumps of the lattice temperature. It may take hours or weeks until the distribution p_Γ of rotor symmetries adopts to the new thermal equilibrium value (2.10) through conversion.

Most of the experimental techniques to obtain temperature-dependent conversion rates use this feature. The oldest results were obtained by measuring the nuclear magnetic susceptibility which is proportional to $\langle \hat{S}^2 \rangle$. The three components of the total (nuclear) spin operator $\hat{S} = \sum_i \hat{s}_i$ are composed of individual spins $\hat{s}_i$ of the identical particles within one rotor. In the cases of the protonated versions of CH_3 or CH_4, a one-to-one relationship exists between the eigenvalue $S(S+1)$ of $\hat{S}^2$ and the symmetry Γ (2.6) [4]. The quantity $\langle \hat{S}^2 \rangle$ can also be determined by measuring the transmittivity of the whole sample for neutrons of wave length's larger than the radius of the rotors as has been found by Hüller and Prager [88]. This established a means to observe conversion over several weeks (magnetic measurements tend to 'drift' after long times) even by using rather weak neutron sources [89, 90] as available e.g. at the PTB Braunschweig [91].

The unique relationship between Γ and S in protonated systems led to call these relaxation processes often 'nuclear spin conversion'. The title of the present

Section 2.2 has been chosen to make clear that it is the symmetry state of the rotor Γ which is the relevant quantum number for energy relaxation processes and not the spin. This is particularly important for deuterated rotors, cf. Section 2.2, where no unique relationship between spins and symmetries exists [92, 93] (cf. (2.6)).

Careful observations of the latent heat that a molecular crystal shows at different cooling rates allows to extract conversion rates at temperatures even slightly exceeding Δ. In a nice recent measurement neutron transmission and specific heat data could be combined to extend the temperature range [94].

The p_Γ can be determined most directly (though also most expensively and in praxis only for sufficiently slow conversion) from the detailed balance factor by measuring the intensities of the inelastic lines in $S(\omega)$. Different types of rotors in the sample showing different tunneling splittings can be distinguished which is a notoriously difficult task for all the above mentioned integral methods. This way the success in preparing purely A-symmetric methane has been demonstrated [95].

The more recent NMR technique using field cycling [96] was the first method not being based on the jump in the lattice temperature. A sophisticated sequence of pulses allows to distort the distribution p_Γ and to monitor its recovery. The required resonance between Δ and the nuclear Zeeman energy restricts the applicability to $\Delta < 0.5\,\mu\text{eV}$. This method is fast compared to all aforementioned techniques so that conversion rates could be observed at temperatures $T \gg \Delta$ for the first time. An Arrhenius type behaviour has been found with an activation energy close to the value expected for Ω.

A very interesting technique has been detected [97, 98] and developed [99, 100] recently to observe conversion of rotors with large Δ and without a priori restrictions to the temperature by optical hole burning using a laser of extremely narrow band width. The method is based on the tiny shift in the energy of an *electronic* excitation of a dye molecule, depending on the symmetry state of the methyl rotor attached to it. The "dynamical" range of accessible conversion rates covers 7 orders of magnitudes. Details about this technique can be found in [99]. For the first time the conversion of the isotopic substitute CD_3 could be observed together with its temperature dependence using this technique [100].

2.2.1 *Protonated rotors*

The first theories to explain symmetry species conversion were designed for the ortho-para transition in hydrogen [101]. It is clear that possible candidates for transition operators must involve the nuclear spin – otherwise the Hamiltonian would still be invariant with respect to the discrete rotations characterizing the rotor type ($\varphi \longrightarrow \varphi + 2\pi/3$ in our favourite example of CH_3). The dipolar magnetic interaction

$$H_{ij}^{\text{DD}} = \gamma^2 \frac{(\boldsymbol{r}_{ij} \cdot \boldsymbol{r}_{ij})(\hat{\boldsymbol{s}}_i \cdot \hat{\boldsymbol{s}}_j) - 3(\boldsymbol{r}_{ij} \cdot \hat{\boldsymbol{s}}_i)(\boldsymbol{r}_{ij} \cdot \hat{\boldsymbol{s}}_j)}{|\boldsymbol{r}_{ij}|^5}$$

suffices to cause symmetry changing transitions. This energy is small due to the smallness of the magnetic moment γ of protons and decreases with the particle distance $\sim |\boldsymbol{r}_{ij}|^{-3}$. In the particular case of H_2 the magnetic intra-rotor interaction still has parity as a symmetry and thus cannot induce conversion. Only ortho-molecules

provide the magnetic field gradient that enables conversion transitions in neighbouring rotors. This inter-rotor interaction mechanism, based on the presence of excited rotors, immediately yields an equation of motion for $p_\Gamma(t)$ being quadratic in p_Γ.

In a general rotational tunneling system $\sum_{ij} H_{ij}^{DD}$ is not invariant with respect to the rotational symmetry of (2.5). Examples are CH_3 and CH_4 rotors. Nijman and Berlinsky [102] established the first theory to explain the conversion in solid methane by *intra-molecular* dipolar interaction (inter-molecular contributions decrease $\sim |r_{ij}|^{-6}$ and are therefore considerably weaker). This interaction by itself still does not provide conversion transitions in isolated rigid rotors where $|r_{ij}|$ is fixed. Only lattice vibrations provide the energy reservoir and allow eventually conversion through "hybrid" processes. The time evolution of $p_\Gamma(t)$ is to a very good approximation determined by a rate equation, linear in p_Γ. This yields the exponential approach $p_\Gamma(t) \sim \exp(-t/\tau_{con})$ towards the equilibrium distribution

$$\bar{p}_\Gamma = tr\{P_\Gamma e^{-H/T} P_\Gamma\}/tr\{e^{-H/T}\} \tag{2.10}$$

at temperature T. The trace refers to the full Hilbert space $\mathcal{H}$ of system plus environment and P_Γ projects onto states in $\mathcal{H}_\Gamma$ with the rotor being Γ-symmetric

$$\mathcal{H} = \bigoplus_\Gamma \mathcal{H}_\Gamma \quad . \tag{2.11}$$

The interesting quantity is the conversion time τ_{con} and its temperature dependence.

The theory [102] is only valid at low temperatures $T < \Delta$ where the conversion rate τ_{con}^{-1} is governed by resonant *"direct"* one phonon processes and therefore proportional to $J(\Delta)$ where $J(\omega)$ is the coupled density of phonon states defined in (2.2). The temperature dependence

$$1/\tau_{con}^{direct}(T) \sim \gamma^4 J(\Delta) \coth(\Delta/2T) \sim \gamma^4 \Delta^3 (1 + 2n(\Delta)) \tag{2.12}$$

is regulated by the Bose distribution function $n(\omega) = (e^{\omega/T} - 1)^{-1}$. Apart from the smallness of the magnetic interaction (its typical energy is still of the order of $\hbar/(10^6\,s)$) the major factor reducing the conversion rate at low temperatures is the small density of phonon states at low energies which additionally is coupled relatively weak to the rotor at long phonon wave length's. The extreme slowness of conversion transitions in methane at low temperatures could be explained satisfactorily by [102].

The repeatedly found correlation between fast conversion and the presence of magnetic impurities [91, 95] is obviously caused by the about 3 orders of magnitudes larger magnetic moment of the electron compared to protons. In this case the hybrid mechanism is not required, the energy can also be provided by the fluctuating distance between rotor and impurity though there is no experimental evidence for noticeable consequences due to the corresponding change in $J(\omega)$. Even dilute magnetic impurities cause fast conversion throughout the sample because of the fast diffusion of symmetry species. No energy transfer is required when two adjacent molecules just exchange their symmetries. This is subject of present research [103].

Already at surprisingly low temperatures $T \gtrsim \Delta$ other processes involving phonons of shorter wave lengths compete and determine the behaviour of $\tau_{con}(T)$. Virtual transitions between librationally excited rotor states start to open additional channels

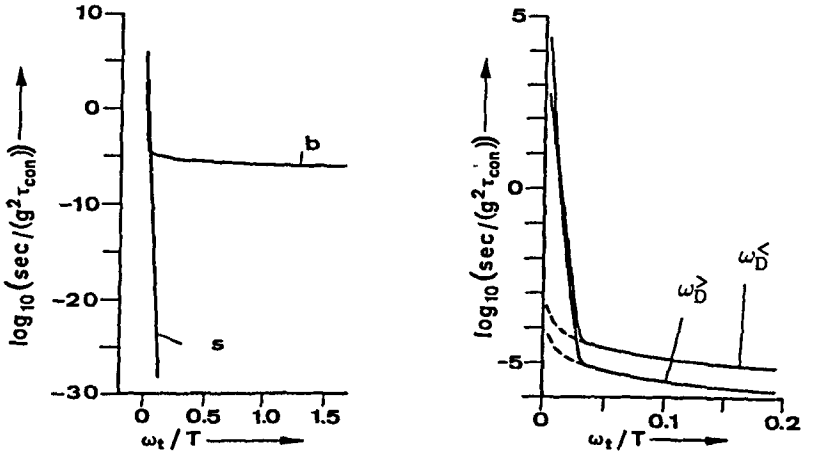

Fig. 7 Conversion rate τ_{con} for a CH_3 rotor in Arrhenius representation ($\omega_t \equiv \Delta$). Coupling to acoustical phonons is assumed, measured by the strength g. Shaking and breathing coupling types are indicated by **s** and **b** respectively. The right figure shows two cases of Debye energies $\omega_D^>$ and $\omega_D^<$ being larger and smaller than the second librational excitation in the lower and upper curve, respectively. The dashed lines were obtained when Orbach processes were ignored.

for conversion [104]. They remind on the *"Orbach process"* [105] known from spin relaxation (T_1-) theory [106, 107]. Perturbation theory with respect to the rotor-phonon coupling leads to the librationally activated Arrhenius type temperature dependence

$$1/\tau_{con}^{orbach}(T) \sim \exp(-\Omega/T) \quad , \tag{2.13}$$

shown in Fig. 7 which is in agreement with experimental observations [108]. The type of phonon coupling, *breathing* or *shaking*, is of crucial importance. The low temperature behaviour (2.12) is completely determined by the former while the activated behaviour (2.13) to appear already at temperatures $T \ll \Omega$ requires the presence of the latter.

This interrelation combined with the opposite shifting behaviour of the tunneling line with temperature (Section 2.1), caused by the two types of phonon couplings, allows the predictions summarized in Table 2. They are in agreement with all known experimental results (cf. [104]).

If additional terms in the rotor-phonon coupling are present being quadratic in the phonon operators $\sim (b_k + b_k^+)(b_{k'} + b_{k'}^+)$ inelastic phonon scattering can occur and compete with the processes leading to (2.12) and (2.13) where only single phonons

Table 2 Relationship between thermal developments of different quantities and the coupling to phonons as predicted within perturbation theory.

Prevailing phonon coupling type	Shifting of tunneling line	Broadening of tunneling line	τ_{con}^{direct} conversion time at low $T \lesssim \Delta$	τ_{con}^{orbach} conversion time at high $T > \Delta$
Shaking	$\delta\Delta < 0$	pronounced	very long	short
Breathing	$\delta\Delta \gtrsim 0$	weak	shorter	longer

were created or annihilated due to H_I. These *"Raman processes"*, again known from spin relaxation theory, lead to the characteristic power law dependence $\sim T^7$ at temperatures $T \ll \Omega$. The conversion rate

$$1/\tau_{con}^{raman}(T) \sim T^7 \tag{2.14}$$

does not depend on Δ [109] but requires a coupling of breathing type [110]. Thus Raman processes lack for somewhat specialized couplings to environmental modes, nevertheless in at least two experimental situations, both associated with large Δ's, such power law dependencies have been observed, one by the neutron transmission method [91], the second, over a wide range of temperatures, by the optical hole burning technique [98, 100, 111]. Precise measurement of conversion rates versus temperatures allows to extract information about the rotor-phonon coupling which is usually difficult to obtain.

2.2.2 Deuterated rotors

The chemical [90, 112] or isotopical [100, 111, 113] substitution of certain atoms can provide extremely useful information about molecular crystals. The crystallographic structure changes only slightly and it may be possible to relate phonon spectra or $J(\omega)$ [113–115] before and after the substitution to one another. Particularly interesting is to replace the hydrogens within the rotors by deuterons. This reduces the rotational constant $B^{(D)} = B^{(H)}/2$ and doubles therefore the heights $V/B^{(D)}$ of orientational potentials measured in units of the corresponding quantum energies. The tunneling energy Δ, depending exponentially on V/B (2.7), is considerably reduced. Also Ω decreases by roughly a factor of $1/\sqrt{2}$ owing to the ratio of masses. Both scaling behaviours are in good agreement with experiments [115].

Predictions about the change in conversion properties require to know the spin states of the rotors which are more complicated for deuterons, being spin $s = 1$ particles, than for protons. For CD_3 the spin states can be found in [103, 113]. The next question addresses the transition operator involving the nuclear spins. It turns out that the electric quadrupolar interaction in CD_3 is about 200 times stronger than the magnetic dipolar interaction between adjacent deuterons [116] (the quadrupol moment of protons is zero). The electric field gradient of strength eq along the C-D bonding, taken as z-direction, yields a quadrupolar energy of the i-th deuteron with quadrupol moment Q

$$H_i^Q = \frac{e^2qQ}{4}(3(\hat{s}_i^z)^2 - \hat{s}_i^2) \quad .$$

To get the transition operator $\sum_i H_i^Q$ one has to rotate the quantization axis' of the three nuclear spins $\hat{s}_i$ parallel to the axis of the rotor. The resulting expression can be found in [110] together with its matrix elements in the basis of the spin states of CD_3.

If $T \gg \Delta$ the temperature dependence of $\tau_{con}^{(D)}$ is again governed by the Orbach process and the conversion times $\tau_{con}^{(D)}$ and $\tau_{con}^{(H)}$ are found to be very much alike when the potential parameters are rescaled accordingly to account for the difference in the hydrogen masses. The products of all collected prefactors turn out to be very similar.

This is approximatively also true for Raman type processes if the rotor is strongly hindered $V \gg B$ (cf. (2.4)). On the other hand valuable information about otherwise unknown quantities can be extracted from the careful measurement of $\tau_{con}(T)$ before and after isotopical substitution if the rotors are almost free $V \lesssim 5B$. In the first experiment two isotopical methyl derivates, embedded in one and the same environment, have been compared [100]. Though the tunneling splitting has not been measured directly (which would be very difficult due to the extremely low concentration of rotors used in the hole burning technique) the changes in the electronic excitation energies of the dye molecule for different rotor symmetries *and* different masses allowed to conjecture the methyl groups to be almost freely rotating. Both conversion times $\tau_{con}^{(H)}(T)$ and $\tau_{con}^{(D)}(T)$ show Raman behaviour at low temperatures which suggests the presence of pronounced quadratic contributions to the rotor-phonon coupling. The conversion of the deuterated species was found to be by almost 2 orders of magnitudes more rapid than the protonated version. If the conversion would be determined by the direct process just the contrary would be expected due to the proportionality $\sim \Delta^3$ of the latter (2.12). The increase of conversion rates with deuteration can be explained when taking into account that the matrix elements of quadrupolar and the dipolar operators differ even qualitatively in the limit of almost free rotors [100, 110]. A quantitative overall picture could be developed explaining all observations. Contrary to previous speculations it could be verified that electronic excitation of the dye molecule increases the orientational barrier for the rotors which can be explained naturally by an increasing size of the dye molecule.

At low temperatures $T \lesssim \Delta$ a qualitatively new behaviour is predicted for $\tau_{con}^{(D)}(T)$ [110] compared to all other theories that appeared yet for symmetry species conversion. The temperature dependence is no longer solely determined from the Bose distribution (2.12) but obeys

$$1/\tau_{con}^{(D)}(T) \sim f(\Delta) = \frac{1 + (16/11)\exp(-\Delta/T)}{1 - \exp(-\Delta/T)} \quad . \tag{2.15}$$

In Fig. 8 the ratio $f(\Delta)/(1 + 2n(\Delta))$ is shown. A similar deviation from the usual behaviour $\sim (1 + 2n(\Delta))$ is expected to appear in the conversion of CD_4 at low temperatures. The experimental proof of both predictions is still lacking.

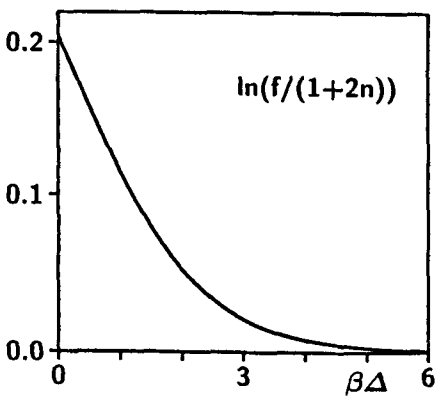

Fig. 8 Relative enhancement of the conversion rate in strongly hindered ($\Delta \ll B$) CD_3 as compared to the behaviour expected for a CH_3 rotor of same tunneling energy Δ in Arrhenius representation. The temperature-dependent function $f(\Delta)$ is defined in (2.15) and $n(\Delta) = (e^{\Delta/T} - 1)^{-1}$ is the Bose function.

In the experiments [100, 111] also methyl rotors composed of intra-molecular isotopic mixtures, like CDH_2, were investigated. The transitions between the low energy states have found to be unobservable fast. This demonstrates beautifully that surrounding fluctuations can now distinguish between the hydrogens and the transitions between the low energy states need no spin-dependent operator. The dynamics of these rotors is not determined by the fundamental identity of particles and they are no rotational tunneling systems in the strict sense.

3 *Correlated few electron systems*

In this part the consequences of particle identity will be investigated for finite systems of strongly correlated electrons. As we shall see this is an important aspect for semiconducting nanostructures, like quantum dots. The single electron effects associated with the charging energy in small conducting structures have been mentioned already in the Introduction. Apart from their fundamental importance for "submesoscopic" devices also possible applications to electronics along the ongoing miniaturization create a high degree of interest in this kind of physics. Contrary to the operation of traditional devices, based on the translational invariance of semiconducting crystals and their band structure the quality of "single electronics", does even improve with reduced length scales at least from the fundamental physics viewpoint [12, 13]. However, many body effects may cause serious complications for the understanding of these systems.

Single electron phenomena and the Coulomb blockade were first observed in small metallic islands [16, 17] where the number of carriers is still in the order of $N \sim 10^8$. The Coulomb interaction can be taken into account in the spirit of a mean field approximation within the so called 'charging model' [117–120] as

$$U \sum_{n_1,\sigma_1,n_2,\sigma_2} c^+_{n_1\sigma_1} c_{n_1\sigma_1} c^+_{n_2\sigma_2} c_{n_2\sigma_2} \tag{3.1}$$

with $U \approx \frac{e^2}{2C}$. The $c^+_{n\sigma}$ create occupation of single electron eigenstates n of the Hamiltonian $\sum_{n\sigma} \varepsilon_n c^+_{n\sigma} c_{n\sigma}$ which describes non-interacting Fermions confined by the external potential. The characteristic feature of the interaction (3.1) is to leave the eigenstates unchanged and to add only an N-dependent additive constant to the energies. The excitation energies are taken as the differences between the single particle energies ε_n. The electron number remains the only dynamical variable of the system [18, 56, 121–123].

Small semiconducting structures, however, showing single electron effects in transport measurements [20, 21, 124–126] or by far-infrared spectroscopy [23, 127] contain considerably smaller numbers of conducting electrons $N \lesssim 100$. Even single electrons $N = 1$ have been realized and observed [23, 127–131] in quantum dots. Semiconducting hetero-structures differ crucially from metallic systems in density and dimensionality ($d = 2$) of the electrons. Therefore correlations and the energies for discrete excitations Δ are considerably enhanced. At temperatures $T < \Delta$ these excitations can be observed by "nonlinear transport spectroscopy" [132–137]. The typical setup has been shown schematically in Fig. 2. Still, if the thermal broadening of the peaks in the differential conductance drops below the life-time broadening related with the finite barrier transmittance, charge fluctuations [122, 123] and effects

arising in higher order in the transmittances (resonant tunneling) [144, 145] and the Kondo effect [138–143] introduce further highly non–trivial complications to the transport theory. These effects will not be considered in the following.

As already mentioned in the Introduction, long-range interactions

$$\sum_{\sigma,\sigma'} \int \mathrm{d}^d x \int \mathrm{d}^d x' \; \Psi_\sigma^+(x)\Psi_{\sigma'}^+(x')w(|x-x'|)\Psi_{\sigma'}(x')\Psi_\sigma(x) \tag{3.2}$$

cause the charge density distribution

$$\langle \varrho(x)\rangle = \sum_\sigma \langle \Psi_\sigma^+(x)\Psi_\sigma(x)\rangle \tag{3.3}$$

of the ground state to 'crystallize'. Here, $\Psi_\sigma^+(x)$ creates an electron at position x with spin σ. For sufficiently large mean electron distances $r_s \gg a_B$ on the length scale of the Bohr-radius $a_B = (me^2/\hbar^2\varepsilon)$ the system minimizes the interaction ($\sim \frac{e^2}{\varepsilon} r_s^{-1}$ for Coulomb forces) on cost of the delocalising kinetic energy $\sim \frac{\hbar^2}{m} r_s^{-2}$ (m and ε are the effective electron mass and the dielectric ratio of the semiconductor). This crystallization has first been predicted by Wigner [27, 146–149] and has been observed for electrons on surfaces of helium [150]. It shows up in the slow decay and the $4k_F$ oscillations of the density-density correlation function

$$g(x-x') = \langle \varrho(x)\varrho(x')\rangle \quad .$$

In reduced dimensionalities $g(x)$ is not truly long range [151–153] ($d = 2$), in $d = 1$ [154] even not at zero temperature, but it decays slower than any power. In electron systems interacting by short range forces (Fermi liquids in $d > 1$ [155], Luttinger liquids in $d = 1$ [156]) or by $w(x) \sim 1/x^2$ (Calogero-Sutherland model [157] in $d = 1$) $g(x)$ decays always algebraically.

In the finite system and in the absence of a continuous symmetry the charges occupy distinguished places inside the dot. This has been presumed for transport calculations through quantum dots [158]. The peak structure of $\langle \varrho(x)\rangle$, see also Fig. 9, motivates the approximation based on localized, correlated pocket state basis functions (cf. Section 3.2).

The N-electron quantum dot is described by

$$\begin{aligned} H &= \sum_{i=1}^{N} \left(\frac{p_i^2}{2m} + v(x_i) \right) + W(x_1 \ldots x_N) \\ W(x_1 \ldots x_N) &= \frac{1}{2} \sum_{\substack{i,j \\ i \neq j}} w(|x_i - x_j|). \end{aligned} \tag{3.4}$$

The x_i and p_i are position and momentum of the i-th electron in d dimensions (mostly $d = 1, 2$). Neither confinement $v(x)$ nor interaction $w(x)$ depend on spin. Therefore, the total spin operator $\hat{S} = \sum_{i=1}^{N} \hat{s}_i$ commutes with H and the energy eigenfunctions are simultaneously eigenfunctions to $\hat{S}^2$ with eigenvalues $S(S+1)$, S being the quantum number for the total spin.

How the Coulomb interaction $w(|\boldsymbol{x}|) \sim e^2/\varepsilon|\boldsymbol{x}|$ influences the many particle excitation spectra has been studied in detail for a harmonic potential $v(\boldsymbol{x}) \sim \omega_0^2 \boldsymbol{x}^2$ in $d = 2$ for spinless electrons [159], and for spin carrying electrons [26, 160] ($N = 2$) and [161] ($N = 3$). Larger electron numbers could be considered by Monte Carlo methods [162]. The case of a rectangle in two dimensions with hard walls has been studied [164] for two electrons. The excitation spectra change qualitatively when ω_0 is reduced or the size of the rectangle increased. Antisymmetrized single particle product states

$$\frac{1}{\sqrt{N!}} \begin{vmatrix} \varphi_1(\boldsymbol{x}_1) & \dots & \varphi_N(\boldsymbol{x}_1) \\ \vdots & \ddots & \vdots \\ \varphi_1(\boldsymbol{x}_N) & \dots & \varphi_N(\boldsymbol{x}_N) \end{vmatrix}$$

ignore correlations and do not suffice to reproduce these spectra [24, 25]. The one-particle states φ_n obey

$$\left[\frac{\boldsymbol{p}^2}{2m} + v + v_{\mathrm{H}}^{(n)} + v_{\mathrm{E}}^{(n)}\right]\varphi_n = \varepsilon_n \varphi_n$$

so that the electrons occupying the states $n' \neq n$ are incorporated in (effective and selfconsistently obtained) mean fields $v_{\mathrm{H}}^{(n)} + v_{\mathrm{E}}^{(n)}$ for 'Hartree' and 'Exchange' contributions

$$(v_{\mathrm{H}}^{(n)}\varphi_n)(\boldsymbol{x}) = \sum_{\substack{n'=1 \\ n' \neq n}}^{N} \int \mathrm{d}\boldsymbol{x}' |\varphi_{n'}(\boldsymbol{x}')|^2 w(|\boldsymbol{x} - \boldsymbol{x}'|)\varphi_n(\boldsymbol{x})$$

$$(v_{\mathrm{E}}^{(n)}\varphi_n)(\boldsymbol{x}) = -\sum_{\substack{n'=1 \\ n' \neq n}}^{N} \int \mathrm{d}\boldsymbol{x}' \varphi_{n'}(\boldsymbol{x})\varphi_{n'}^*(\boldsymbol{x}')w(|\boldsymbol{x} - \boldsymbol{x}'|)\varphi_n(\boldsymbol{x}').$$

This optimal mean field (Hartree-Fock) approximation favours spin polarized ground states at low densities [165, 166] which already contradicts to the fact that the ground state of two interacting electrons can strictly shown to be a singlet $S = 0$ in any dimensions [167].

The charge density distributions of ground states shown in Fig. 9 belong to the square well potential in $d = 1$

$$\begin{aligned} v(x) &= V_0 \Theta(|x| - L/2), \qquad V_0 \gg \pi^2 N^2/mL^2 \\ w(x) &= \frac{e^2}{\varepsilon} \frac{\mathrm{e}^{-\alpha|x|}}{\sqrt{x^2 + \lambda^2}}, \qquad \lambda \ll L \end{aligned} \tag{3.5}$$

of size L. The cutoff length's at small and at large distances, λ and α^{-1}, simulate a (small) transversal spread of the wave functions and the influence of screening, respectively. The numerical diagonalizations for $N \leq 4$ electrons have been performed in the basis of eigenstates of the corresponding Hamiltonian in the absence of interactions. For most of the results the lowest $1 \leq n \leq M = 13$ single electron states were

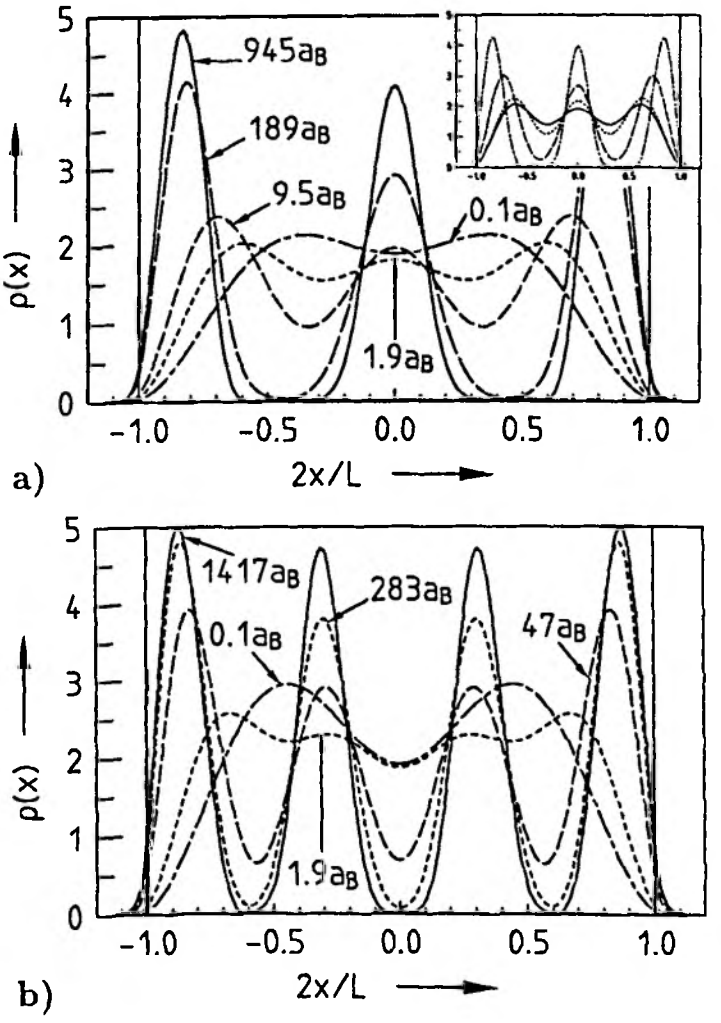

Fig. 9 Charge density $\varrho(x)$ of (a) $N = 3$ and (b) $N = 4$ electrons in the ground state of a 1D square well potential of depth V_0 for different L [28] ($\varrho(x)$ in units of $2N/L$).
The inset in (a) [163] shows $\varrho(x)$ for different $\alpha = 0, 0.007, 0.1, 1, 10\ a_B^{-1}$ in dot-dashed, dashed, dotted, and solid at fixed $L = 1417\ a_B$. The last two cases are not distinguishable in the figure.

included. The occupation number representation, including spin, yields Hamiltonian matrices of rank $\binom{2M}{N}$, being equal to 14950 in the largest case. The matrices contain to a high percentage zeros, only entries are non-vanishing with rows and columns differing at most in two occupation numbers. The sparsity of the matrix and our interest in only the lowest eigenstates makes use of Lanczos procedures advantageous. Particular symmetries of the matrix elements are discussed in [168] and the calculational details can be found in [28, 168–170].

3.1 Numerical results

3.1.1 Ground state properties

Figure 10 shows the dependence of the ground state energy per particle E_0/N on the particle number N for different L. The data are multiplied by L to eliminate the triv-

ial L-dependence. The charging model (3.1) would yield a straight line in this plot. At high densities E_0/N deviates from a linear N-dependence due to the kinetic energy contribution. But also at low densities r_s^{-1} the ground state of few electrons fails to obey $E_0/N \propto (N-1)$ owing to the formation of an inhomogeneous charge density distribution (Wigner molecule). The Coulomb energy of N point charges at equal distances $r_s = L/(N-1)$ provides a better approximation (crosses in Fig. 10).

The influence of charge "crystallization" on the capacitance per unit length C/L can be demonstrated for equidistant point charges e in 1D

$$\langle \varrho(x) \rangle = e \sum_{j=1}^{N} \delta(x - x_j) \quad , \quad x_j = \frac{j-1}{N-1} L \quad .$$

The capacitance, defined as

$$C(N) := (Ne)^2/2U$$

where

$$U = \sum_{\substack{i,j \\ i \neq j}} \frac{e^2/\varepsilon}{|x_i - x_j|} = \frac{e^2}{\varepsilon L}(N-1) \sum_{j=1}^{N-1} \frac{j}{N-j} = \frac{e^2}{\varepsilon L} N(N-1) \sum_{j=2}^{N} \frac{1}{j} \tag{3.6}$$

is the charging energy, does depend on the total charge Ne

$$C(N)/\varepsilon L = \frac{N}{2(N-1)} \left[\sum_{j=2}^{N} \frac{1}{j} \right]^{-1}$$

which is in contrast to the classical capacitance of a homogeneously charged and long cylinder. The classical relationship between voltages and charges becomes inapplicable already due to the granular nature of the charges. This argument applies also to higher dimensions. Considerable fluctuations of small capacitances with the charge are expected at low densities [171].

If, on the other hand, the kinetic energy contribution becomes comparable to the charging energy in very small dots [127] ($\frac{r_s}{a_B} < \left(\frac{N}{N-1}\right)^2 \frac{1}{\ln N - 1 + C}$, C: Euler constant) the ground state energy again cannot be approximated well by the capacitance formula. This situation seems not yet reached in the present nanostructures used in transport experiments [20, 22, 124]. There $r_s \approx 3\, a_B$ can be estimated from the dot area and the electron number which makes the charging model reliable to guess the *ground state energy* being relevant for linear transport experiments. However, the *excitation energies* are considerable-different from the ones expected within the non-interacting picture as will be explained below. They are importantly characterized by the spin.

The exact charge density distributions, shown in Fig. 9, confirm this view. Similar results have also been obtained in the presence of a strong magnetic field [172]. Three regimes of electron densities can be distinguished. For $r_s \lesssim 0.1\, a_B$ the spectrum is dominated by the kinetic energy and the Coulomb interaction is only a weak perturbation in (3.4) so that $\langle \varrho(x) \rangle$ is basically determined by the lowest occupied single particle states. This causes the minimum at $x = 0$ (Fig. 9). At $r_s \gtrsim a_B$, $\langle \varrho(x) \rangle$ changes

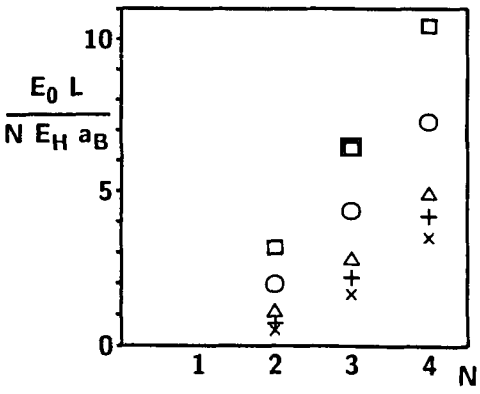

Fig. 10 Ground state energies per particle E_0/N multiplied by L/a_B versus the particle number N for $L = 6.61\,a_B$ (□), $L = 16.1\,a_B$ (○), $L = 94.5\,a_B$ (△), $L = 944.8\,a_B$ (+). (×) denote the energy of N fixed point charges equally spaced at distances $L/(N-1)$. The quantum mechanical ground state energies approach these values as $L \to \infty$.

qualitatively and N peaks start to emerge. The "critical" length is of the same order as found in [168] for the crossover from an almost non-interacting energy spectrum into the spectrum composed of level-multiplets. When r_s increases further, say $r_s \gtrsim 100\,a_B$, $\langle \varrho(x) \rangle$ vanishes almost completely between the maxima indicating a fully established Wigner molecule. In this limit the ground state energy can be approximated reasonably well by that of a chain of static elementary charges at equal distances r_s (3.6).

In order to investigate the influence of the long range part of the Coulomb interaction, an exponential cutoff $V(x,x') \propto e^{-\alpha|x-x'|}/\sqrt{(x-x')^2+\lambda^2}$ at distances α^{-1} has been introduced in the 1D system (3.5). In the inset of Fig. 9 a $\langle \varrho(x) \rangle$ is shown for different $\alpha \neq 0$. Despite of the considerably reduced range of the interaction pronounced maxima are obtained. However, compared to $\alpha = 0$ the distribution rather resembles a charge density wave [147] than a Wigner molecule. The long range part of the Coulomb interaction is essential to yield long range density-density correlations [154]. Screened interactions $\alpha^{-1} < r_s$ finally make mean field approximation for the ground state energy within the charging model reliable, even at low densities.

3.1.2 Excitations

In the 'crystallized' limit $r_s \gg a_B$ vibrations of the localized electrons around their equilibrium positions determine the phonon-like (cf. [152, 153]) low energy excitations. The system resembles a (finite) harmonic chain. Restricting the forces to nearest neighbours, the highest and the lowest phonon frequencies can be estimated for $N > 3$ by

$$\Omega_{\max} = 2E_H \left(\frac{a_B}{r_s}\right)^{3/2}$$
$$\Omega_{\min} = \frac{\pi}{2}\frac{1}{N-2}\Omega_{\max} \tag{3.7}$$

where $E_H := e^2/\varepsilon a_B$ equals twice a Rydberg. Figure 11 shows the numerically obtained Ω multiplied by the system length's L versus r_s for $N = 2, 3$. The behaviour is well described by the power law dependence $\Omega r_s \sim r_s^{-1/2}$ (3.7) at $r_s \gtrsim 100\,a_B$.

Also for $\alpha > 0$ power law behavior $\Omega \sim r_s^{-2}$ is recovered, though with the exponent changed from 3/2 to 2 [28]. This is explained by the almost free motion of the electrons if $\alpha r_s \gg 1$ within an interval of the length r_s.

The phonon-like excitations do not depend on the spin of the particles. Fermions and Bosons show the same spectrum at lowest densities. For spin half particles the states are 2^N-fold degenerate. Pronounced deviations from the asymptotic behavior at elevated densities signalize the breakdown of the Wigner molecule. The spin degeneracy is partly lifted and each vibrational level reveals a fine structure shown schematically in Fig. 12. The latter exhibits the systems' smallest excitation energies Δ in this regime of intermediate electron densities. The individual eigenstates differ in their total spins $S = \begin{Bmatrix} 0 \\ 1/2 \end{Bmatrix}, \ldots, N/2$ for $N = \begin{Bmatrix} \text{even} \\ \text{odd} \end{Bmatrix}$ though a given spin S may appear more than once in the multiplet. Group theory allows to connect the behaviour of the eigenfunctions under coordinate transformations with a certain spin S, see Section 3.3. For $N \geq 3$ the states are in general not products of a spatial and a spin part [59].

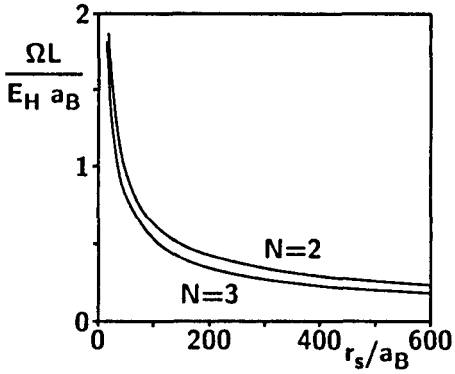

Fig. 11 Energy difference Ω between the two lowest multiplets of energy levels, multiplied by L/a_B versus the mean particle distance r_s for $N = 2$ and $N = 3$.

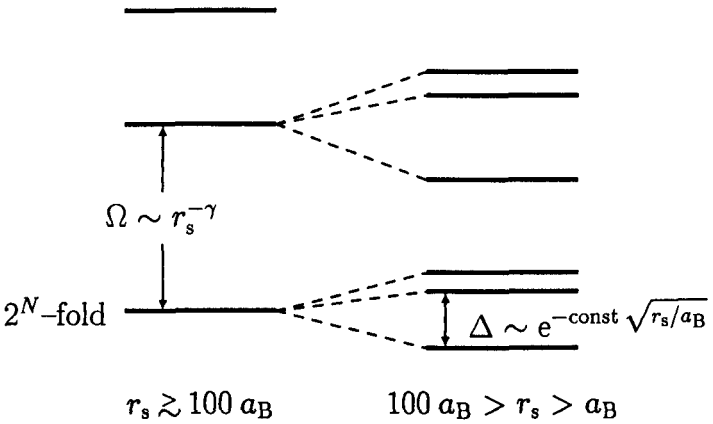

Fig. 12 Scheme of the energy levels of a few strongly interacting electrons. The phonon-like excitation energies Ω of the Wigner crystal at large r_s ($r_s \gtrsim 100\, a_B$) do not depend on spin. The levels are 2^N-fold degenerate (left). With decreasing r_s they split (right) because of tunneling between equivalent electron configurations. In the absence of spatial symmetries each sublevel can be labeled only by the total electron spin S.

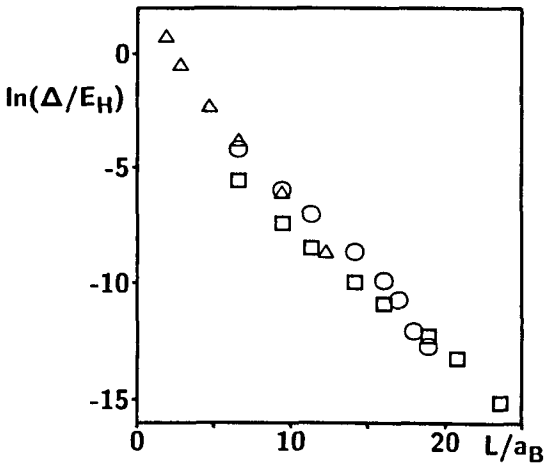

Fig. 13 Logarithm of the energy difference Δ between the ground state and the first excited state within the lowest multiplet versus the system length for $N = 2$, $M = 11$ (□), $N = 3$, $M = 13$ (○), and $N = 4$, $M = 10$ (△).

The fine structure splittings will be determined quantitatively in Section 3.4 using the pocket state method. The low energy excitations will be related to processes of electrons interchanging their places in the Wigner molecule-like configuration by tunneling through the Coulomb barrier. These energies scale roughly exponentially $\Delta \sim \exp(-\sqrt{r_s/r_c})$ with the mean electron separation r_s (see Fig. 13). Sufficiently low electron densities $r_s^{-1} \ll r_c^{-1}$ enable the condition $\Delta \ll \Omega$ which is required for the pocket state method to be valid. The scale r_c separates the regimes of weak and strong interactions, the latter being characterized by the existence of level-multiplets. The fine structure reflects quantum corrections to the Wigner crystallized limit [173]. At further increased densities descriptions like the Luttinger liquid ($d = 1$) or the Hartree-Fock approximation ($d > 1$) can be used.

The one-dimensional case (3.5) is in so far special compared to higher dimensions as no truly long-range interaction ($\alpha = 0$) is necessary to provide $\Delta \ll \Omega$ in finite systems at low densities. The barriers between the equilibrium electron positions are not destroyed, although their thickness (of order α^{-1}) is reduced compared to the Coulombic limit [28]. The low energy excitations can still be described as quantum corrections to crystallized electrons, just slightly larger r_s are needed. In higher dimensions an interaction $\sim r_s^{-\gamma}$ with $\gamma < 2$ is essential to keep the electrons apart from one another and to maintain $\Delta \ll \Omega$.

3.2 Pocket states

In the absence of explicit spin dependencies the eigenenergies of Hamiltonians like (3.4) depend only on spatial space properties. The corresponding eigenfunctions are solutions of a differential equation under appropriate boundary conditions. For convenience we will ignore in the following the identity and the spin of the particles and consider only spatial space. This increases the Hilbert space by the not necessarily (anti-) symmetric functions. The corresponding extra eigenvalues, however, do not appear in the physical system and in Section 3.3 the true Fermionic or Bosonic eigenvalues will be recovered by considering then the spin. For the moment the Hamiltonian (3.4) is conceived as describing *one* particle in a space of $N \cdot d$ dimensions.

In $d = 1$ (3.5), the configuration space for this particle is given as a (hyper-) cube L^N. The repulsive interaction W creates potential barriers (at least of height e^2/λ) that separate $N!$ minima of the total potential $\sum_i v(\boldsymbol{x}_i) + W$. Due to particle identity, the minima are precisely equivalent and their locations are related to each other by permutations of coordinates. In the 2D case additional symmetries may create a multiple of $N!$ of minimas. This latter case will be discussed in Section 3.5. In configuration space the minima are located on a hyper-ring (i.e. a $(N-2)$-dimensional manifold) perpendicular to the main diagonal of the cube L^N so that the center of the ring coincides with the center of the cube. Every minimum is surrounded by $N-1$ nearest neighbouring minima at equal distances.

A very suitable approximation for the low energy properties is best explained for the example of a symmetric double well potential $V(x) = V(-x)$ in one dimension, as it is sketched in Fig. 14. The Hilbert space is restricted to the two "pocket" states $|L\rangle$ and $|R\rangle$, each being peaked around one minimum of V. Both states are related to one another by mirror symmetry $\langle x|L\rangle = \langle -x|R\rangle \geq 0$. Within this approximation the ground state is given as the symmetric, the first excited state as the antisymmetric linear combination of both basis functions. The energy difference Δ between the associated eigenvalues is proportional to the off-diagonal entry $\langle L|H|R\rangle$. It equals the frequency for tunneling between the left and the right state. This approximation is good for sufficiently high barrier between both potential minima to provide

$$\Delta \ll \Omega \tag{3.8}$$

where Ω is the energy of higher excitations in the double well. The corresponding higher excited states have nodes near the potential minima and cannot be approximated within the two state basis $\{|L\rangle, |R\rangle\}$.

The exponential decay of $\langle x|L\rangle$ and $\langle x|R\rangle$ in the classically forbidden region causes the overlap $\langle L|H|R\rangle = \Delta/2$ to decrease exponentially with increasing distance r between the minima. Furthermore, $\Delta \sim \exp(-\lambda^{-1/2})$ with increasing height λ^{-1} of the barrier. Due to the only algebraic decay of Ω with r for all non-pathological interactions, (3.8) is fulfilled at sufficiently large r and the truncation of the Hilbert space to span $\{|L\rangle, |R\rangle\}$ is justified at low energies.

The problem of Section 3.2 can be treated in a similar spirit. The pocket state approximation (PSA) is not limited to one-dimensional or translationally invariant potentials as it has been demonstrated for rotational tunneling systems [4, 7]. It consists in truncating the Hilbert space to span $\{|p\rangle\}$ of $1 \leq p \leq N!$ states, the amplitude $\langle x_1, \ldots, x_N|p\rangle$ of each being strongly peaked around one certain potential minimum and small elsewhere. The elements of the Hamiltonian matrix $\boldsymbol{H}$

$$H_{pp'} \equiv \langle p|H|p'\rangle$$

describe *correlated* tunneling between two different *arrangements* p and p' of the N particles. The basis states $|p\rangle$ are not given as single particle products and account for correlations. The ground state has the same symmetry as the Hamiltonian and is given by the linear combination

$$\frac{1}{\sqrt{N!}} \sum_{p=1}^{N!} |p\rangle. \tag{3.9}$$

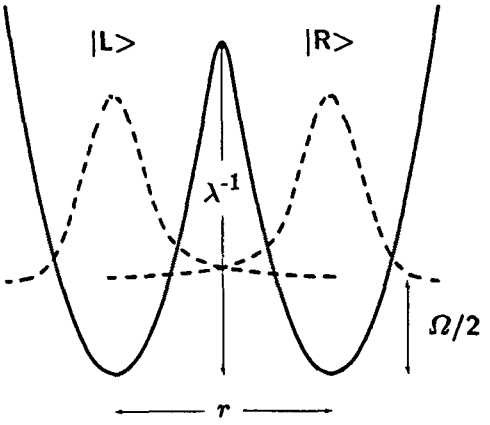

Fig. 14 Double minimum potential, schematically. If $\langle L|H|R\rangle \ll \Omega$ the Hilbert space can be restricted to span $\{|L\rangle, |R\rangle\}$ to describe the lowest excitation.

The inhomogeneous charge density distribution

$$\rho(x) = \frac{1}{(N-1)!}\sum_{p,p'}\int \mathrm{d}x_2 \ldots \mathrm{d}x_N \; |\langle x, x_2 \ldots, x_N|p\rangle\langle p'|x, x_2 ..., x_N\rangle, \qquad (3.10)$$

obtained in [28], reflects the separation of different probability amplitudes $\langle x_1, \ldots, x_N p\rangle$ and $\langle x_1, \ldots, x_N|p'\rangle$.

Within reasonable (WKB) approximations one can show [174] that the whole lowest level-multiplet is determined by just one parameter which is the off-diagonal $H_{pp'}$ with largest modulus. All energy differences are proportional to this parameter so that the ratios between the excitation energies do not depend on the precise form of the electron-electron interaction potential w.

The lowest of the vibrational excitations which equals the separation between the lowest two level-multiplets is related to the collective motion of all particles in phase (acoustic mode). It decreases $\sim 1/(N-1)$ with increasing N if r_s remains constant. This restricts the pocket state description to systems of finite sizes. In the thermodynamic limit the acoustic mode evolves into the zero energy Goldstone mode so that (3.8) is violated and the low energy spectrum is no longer determined by well separated multiplets.

3.3 Symmetries

Appropriate use of symmetries facilitates understanding and computation of eigenstates and transition rates [175, 176]. Since the Hamiltonian commutes with the elements of a symmetry group, its eigenfunctions transform according to the irreducible representations (IR) Γ of this group. The Hilbert space $\mathcal{H}$ of wave functions can be decomposed into orthogonal subspaces $\mathcal{H}_\Gamma$

$$\mathcal{H} = \bigoplus_\Gamma \mathcal{H}_\Gamma \qquad (3.11)$$

so that the Hamiltonian matrix in a symmetrized basis is block diagonal. This can considerably simplify numerical diagonalizations. The property (3.11) is mostly ap-

plied to single particle states, as they are obtained e.g. within molecular field approximation for instance in calculations of band structures or molecular orbitals. Here (3.11) is applied to the pocket state basis to select the appropriate eigenvalues from the spectrum obtained in Section 3.2 that are in accordance with the Pauli principle for identical, spin carrying Fermions or Bosons.

The indistinguishability of like particles requires that any eigenfunction of (3.4)

$$\psi(\boldsymbol{x}_1\sigma_1,\ldots,\boldsymbol{x}_N\sigma_N)$$

belongs to the one-dimensional (anti)symmetric IR of the group of permutations S_N [177] regarding the *enumeration* of the N particles. These permutations affect position $\boldsymbol{x}_j$ and spin σ_j of each particle simultaneously.

Apart from this unalienable symmetry the Hamiltonian (3.4) is additionally invariant under *separate* permutations of the $\{\hat{\boldsymbol{x}}_1,\ldots,\hat{\boldsymbol{x}}_N\}$ and $\{\hat{\sigma}_1,\ldots,\hat{\sigma}_N\}$ operators if spin–orbit coupling is absent. Therefore ψ can further be classified according to the IR's Γ_x and Γ_σ of the group of permutations among the spatial and the spin degrees, respectively, cf. (1.2) and (1.3). Both permutation groups are isomorphous to S_N.

One can show that for spin 1/2-particles Γ_x and Γ_σ are related to each other, $\Gamma_x = \Gamma_\sigma$ for Bosons and $\overline{\Gamma}_x = \Gamma_\sigma$ for Fermions. $\overline{\Gamma}$ denotes the to Γ adjoined IR of S_N [2]. Furthermore, Γ_x and Γ_σ both are uniquely fixed by the total spin $S = \left\{\begin{smallmatrix}0\\1/2\end{smallmatrix}\right\},\ldots,N/2$ the N spins are coupled to [174].

3.4 Results for 1D quantum dots

For low electron numbers the individual blocks of the Hamiltonian matrix in the symmetrized basis according to (3.11) can be diagonalized analytically, in 1D up to $N \leq 4$. The results are given in Table 3 in units of the largest overlap matrix element $\max_{p\neq p'} |H_{pp'}| \equiv t_N$. Fine structure spectra for $N = 5$ and $N = 6$, shown in Fig. 15, are obtained by numerical diagonalization of blocks of sizes 25×25 and 81×81, respectively. The diagonalization of the full Hamiltonian in the basis of non-interacting electrons, as carried out in [168], was possible only for $N \leq 4$ to include a sufficient number of single particle levels and obtain accurate fine structures. The rank of the matrices were in the order of $10^4 \times 10^4$. These data are included in Fig. 15. Not only the sequence of spin values is described correctly within PSA but also the quantitative ratios between the level separations.

Lieb and Mattis [167] have proven the ascending order

$$E(S) > E(S') \quad \text{if} \quad S > S' \tag{3.12}$$

of the lowest energy eigenvalues $E(S)$ to given spins S for a one-dimensional electron system. No further restrictions for the interaction $w(x)$ between the electrons are required but boundedness and independence of spin. Consequently the ground state is either of $S = 0$ or of $S = 1/2$. All fine structure spectra shown in Fig. 15 obey (3.12).

It can further be shown that the state with polarized spins $S = N/2$ is of highest energy within the lowest multiplet [174]. This property resembles a Heisenberg chain of anti-ferromagnetically coupled spins and is an indication for the relationship between quantum dot electrons and the Hubbard model, here at half filling, in the absence of any underlying potential lattice [32]. The $S = N/2$ state plays a distin-

Table 3 Analytical values for the fine structure spectrum $E_i^{(N)}$ of model (3.5) within PSA for $N \leq 4$. S refers to the total spin of N Fermions with $s = 1/2$. The excitation energies $E_i^{(N)} - E_{\text{Bose}}^{(N)}$, in units of t_N, refer to the eigenvalue $E_{\text{Bose}}^{(N)}$ of the symmetric linear combination of pocket states (3.9) corresponding to the $s = 0$ Bosonic ground state.

N	S	$E_i^{(N)} - E_{\text{Bose}}^{(N)}$
2	0	0
2	1	$2t_2$
3	1/2	t_3
3	1/2	$3t_3$
3	3/2	$4t_3$
4	0	$(3-\sqrt{3})t_4$
4	1	$(4-\sqrt{2})t_4$
4	1	$4t_4$
4	0	$(3+\sqrt{3})t_4$
4	1	$(4+\sqrt{2})t_4$
4	2	$6t_4$

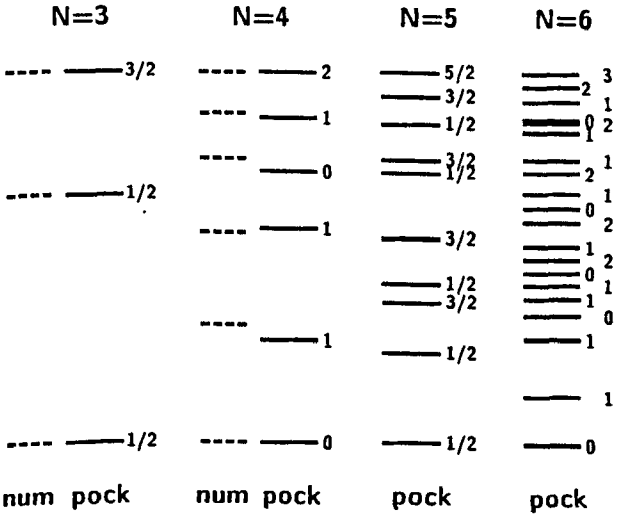

Fig. 15 Fine structure multiplets for $N = 3, \ldots, 6$ as obtained within PSA (pock). Numerical results (num) (dashed) have been obtained [168] for systems of length $L = 11.3\, a_B, N = 3$ and $L = 13.2\, a_B, N = 4$. The energy scale t_N has been adjusted to normalize the overall width of the multiplets. No numerical results are available for $N = 5, 6$.

guished role for the transport through a quantum dot at finite applied voltages – it causes negative differential conductances [8]. Calculations restricted to spinless Fermions yield this state as ground state. The spin degree of freedom allows the interacting electron system to lower its ground state energy. A similar result has been found recently also for the 3D Wigner crystal [178].

3.5 Results for 2D quantum dots

Also finite systems of higher dimensionalities show well separated peaks in the one particle distribution at low densities if continuous symmetries are absent. Then the lowest spin involving excitations can again be described using pocket states. The spectrum shows vibrational levels which are split due to tunneling between different

electron arrangements, similar to the 1D case. The important difference to 1D are the reduced heights of the potential barriers separating the configurations so that the electrons can interchange their positions more easily by surrounding each other. Some of the corresponding paths involve just slight changes of electron distances, so that the tails of the long range Coulomb interaction creates only shallow barriers between the locations of the potential minima. The PSA would fail if $w(x)$ was only short range. Furthermore, the PSA requires electron distances r_c larger than in 1D to provide sufficiently small kinetic energies. Then, however, the scaling behaviours $\Delta \sim \exp(-\sqrt{r_s/r_c})$ of the spin sensitive and $\Omega \sim r_s^{-\gamma}$ of the vibrational excitations are still different, and $\Delta \ll \Omega$ will be established at sufficiently large r_s.

The two-dimensional case applies to most experimental situations. Numerical results for excitation spectra of Coulombically interacting electrons in rectangular, hard wall quantum dots [179] at low electron densities are available only for $N = 2$ [164]. Figures 1 and 2 of [164] confirm the expected grouping of the levels with increasing system size L into vibrational multiplets with internal structure. A considerably larger value for r_c compared to $1.7\,a_B$ can be estimated from these Figures.

The striking similarities between vibrational and fine structure excitations of two electrons in a 2D hard wall rectangle of length L and width $L/10$ (Fig. 1 in [164]) and the corresponding spectrum for a 1D square wall box (Fig. 1 in [168]) becomes understandable in view of the large width u of the pocket state wave function compared to the width of the rectangle. In the narrow system [164] u would be estimated in terms of Airy functions by linearizing the interaction $e^2/\varepsilon(x - r_s)$ for $x \ll r_s$

$$\frac{u}{a_B} \approx \frac{1}{2}\left(\frac{21}{4}\pi\right)^{2/3}\left(\frac{r_s}{a_B}\right)^{2/3}$$

to be larger $u \gtrsim L/10$ than the width of the rectangle as long as $r_s = L < 3 \times 10^4\, a_B$. Then transversal excitation energies $\sim \pi^2(10/L)^2$ still exceed longitudinal vibrational or fine structure excitations. The system is quasi one-dimensional and its spectrum can be approximated by putting $\lambda/L = 0.1$ in (3.5). Systems of larger sizes have not been considered in [164] where differences might appear.

To understand the spectrum for two electrons in a hard wall square, Fig. 2 of [164], within PSA the method described in Section 3.2 has to be generalized. The substitutional single particle (Section 3.2) moves now in the configuration space L^{2N}. The number of potential minima may be a multiple ν of $N!$ if there exist ν energetically equivalent classical electron configurations for the repulsively interacting electrons. This is the case e.g. for $N = 2$ where $\nu = 2$.

The 4 pocket states for two electrons in a square are illustrated in Fig. 16a). The dominant overlap integrals between them are of the type $\langle 1|H|2\rangle = \langle 1|H|3\rangle$. Due to the longer tunneling path overlap integrals like $\langle 1|H|4\rangle$, which corresponds to the exchange of the positions of two like particles, are much smaller. Neglecting the latter and classifying the obtained eigenstates according to their transformation properties with respect to *permutations among the particle enumeration* leads to a fine structure spectrum as shown in Fig. 16 b). The multiplet contains in total $\nu \cdot 2^N$ states (including Zeeman degeneracies). The ground state is a symmetric linear combination of the 4 pocket states and its one particle density (3.10) shows 4 peaks of equal weights in the 4 corners, each containing a charge $e/2$. Removal of the square symmetry (cf. Section 4) would cause the two degenerate $S = 1$ states to split.

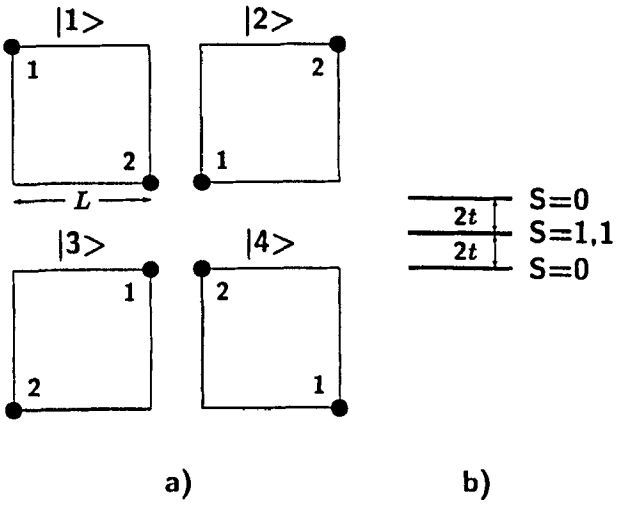

Fig. 16 a) The 4 equivalent arrangements of minimal repulsion between $N = 2$ electrons on a square that form the 4 pocket states in L^4. b) The resulting fine structure spectrum consists of 3 levels at equal distances and total spins S as indicated.

Three classical electrons are again preferably located in the corners of the square in $\nu = 4$ possible ways so that tunneling into the empty place is the dominant quantum process. The fine structure multiplet is determined by $4 \cdot 3! = 24$ pocket states. Considering only the dominant overlap integral yields the spectrum shown in Fig. 17. There are in total $4 \cdot 2^3 = 32$ states in the multiplet.

Four and five electrons in a square have only $\nu = 1$ classical ground state configuration. The number of pocket states is 4! and 5!, respectively. For $N = 5$ the dominant tunneling process is the exchange of the central electron with an electron situated at one of the corners. The corresponding path is of shortest length and involves only 2 electron masses. For $N = 4$ it is not so obvious which of the two possible paths for transitions between different arrangements of the electrons, one being located at each corner, yields the larger tunneling integral: *i*) the rotation of all four electron positions simultaneously by 90° (ring exchange). *ii*) the exchange of just two adjacent electrons leaving the remaining two unaffected. In one case the mass and in the other case the height of the potential barrier is larger. Within WKB approximation a slight dominance of process *ii*) is found [174]. Neglecting all other processes leads to a fine structure spectrum for four electrons as it is shown in Fig. 17. However, the difference between the two paths is not very pronounced so that entries due to the ring exchange into the Hamiltonian matrix can modify the $N = 4$ fine structure if $r_s = L$ is not very large.

A prominent property of the correlated eigenstates obtained in 2D are values of ground state spins, which, in contrast to 1D, are not the lowest possible ones. The three electron ground state is spin polarized and the five electron ground state has spin $S = 3/2$. The Lieb and Mattis Theorem cannot be generalized to higher dimensionalities if $N > 2$. The values for the ground state spins influence crucially both the linear and the nonlinear transport behaviour of 2D quantum dots [180].

Cases with larger electron numbers can, in principle, be treated analogously, provided $\Delta \ll \Omega$ is satisfied. With increasing N this requires a decreasing electron density because:

1. the vibrational energies $\Omega \sim 2\pi e/(N-1)^{1/d}\sqrt{\varepsilon m r_s^3}$ decrease with increasing size of the system due to acoustic modes

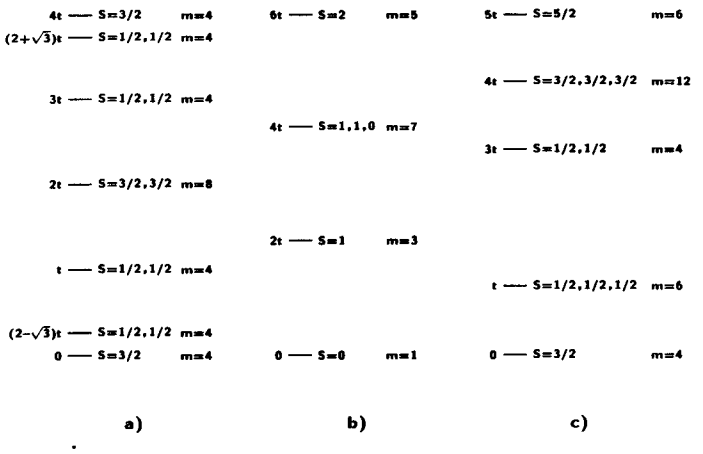

Fig. 17 Multiplets for **a)** $N = 3$, **b)** $N = 4$, **c)** $N = 5$ electrons in a 2D square as obtained using the PSA (S total spin, m degeneracy of the levels).

2. the barriers between equivalent electron arrangements decrease so that Δ increases (cf. [28]).

The first point depends only on the electron density while the second point makes the pocket state approximation less reliable for instance in three-dimensional situations.

3.6 Nonlinear transport

The at present most complete experimental access to the properties of the many body states in quantum dots are linear and nonlinear transport measurements. Apart from the Coulomb blockade effect which is also known from metallic islands, where the current vanishes for small transport voltages if the extermally applied chemical potentials $\mu_L = \mu_R$ are not equal to the difference $E_0^{(N)} - E_0^{(N-1)}$ between ground state energies of adjacent electron numbers, new features appear for strongly correlated situations in quantum dots which are related to the electron spin.

Finite transport-voltages $V = (\mu_L - \mu_R)/e$ involve additionaly transitions between states of excited energies $E_i^{(N)}$ and $E_j^{(N-1)}$. The current jumps step-wise with changing voltages at zero temperature. These features make the spectrum $E_i^{(N)}$ of the dot indirectly visible. Increasing transport-voltage, however, may decrease the current!

The occurrence of negative differential conductances has been investigated in detail experimentally [132, 136]. Theoretically [8, 180–183] they were traced back to spin selection rules ('spin blockade'). An entering or escaping electron is able to change the total spin of the correlated dot electrons only by $\pm 1/2$.

The decreasing current can be explained already within a rate equation approach for the transport which is valid only if interferences between subsequent electron passages can be neglected [144], e.g. at temperatures larger than the rate for electron passages, $T > \Gamma$. Too transmissive barriers or extremely weak incoherencies of the many electron wave functions inside the dot require to take into account the time evolution of the full density matrix [184] in order to recover the Kondo features [138–143] or resonant tunneling [144, 145, 186, 187]. The stationary, nonlinear current

$$I = (+/-)e \sum_{ij(i\neq j)} P_j \Gamma_{ij}^{L/R} \Delta N \tag{3.13}$$

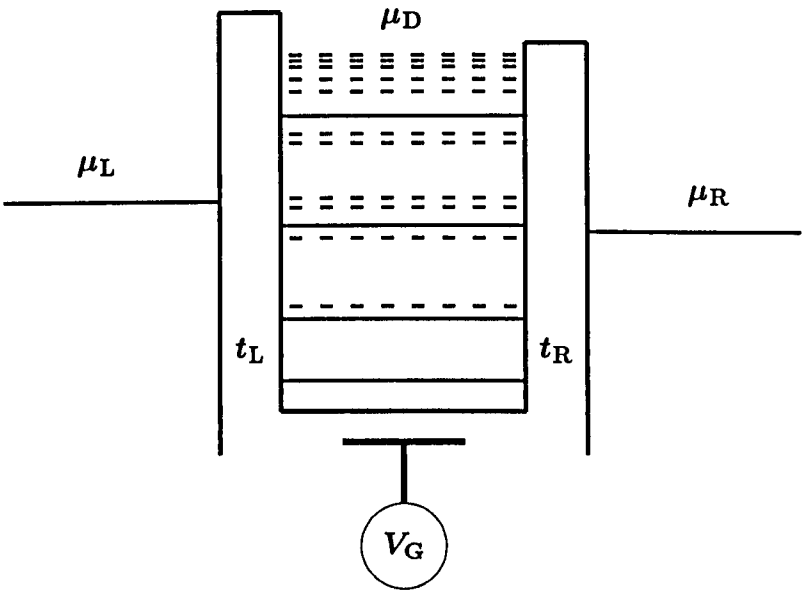

Fig. 18 Quantum dot connected to electron reservoirs by small transmittances t_L and t_R. The dot potential can be adjusted by V_G. When quantum fluctuations of the electron number inside the island can be ignored, the transport vanishes if the difference between the ground state energies $E_0^{(N)} - E_0^{(N-1)}$ (solid lines) lies not between the external chemical potentials. At finite transport voltages $V = (\mu_L - \mu_R)/e$ and at low temperatures the differences $E_i^{(N)} - E_j^{(N-1)}$ (dashed) between discrete excitation energies of the quantum dot can be observed. The level differences move up and down with V_G.

is determined by the rate for electron passages through either of the two barriers $\Gamma^{L/R}$, changing the dot electron number by $\Delta N = \pm 1$, and by the stationary nonequilibrium populations P_i which obey

$$\sum_{i(i\neq j)} (\Gamma_{ij} P_j - \Gamma_{ji} P_i) = 0 \quad , \quad \sum_i P_i = 1 \quad . \tag{3.14}$$

The index **i** refers to the many electron dot levels (in Fock space) [8, 181, 183] which includes (i) the electron number N, and at given N (ii) the total spin S, (iii) its (Zeeman-) z-component and (iv) the energy.

The $\Gamma_{ij} = \Gamma_{ij}^L + \Gamma_{ij}^R$ denote the rate for transitions from state **j** to state **i**, either due to the entrance or the escape of one single electron (simultaneous two-electron passages are suppressed for weak dot-lead coupling). They are proportional to the transmittances $t_{L/R}$ of the barriers. For simplicity the $t_{L/R}$ are assumed not to depend on energy. Electron passages through either of the barriers are stochastically independent. The Γ_{ij} also guarantee energy conservation and depend on the Fermi distributions for the occupied lead states (which depend on temperature and transport voltage). The gate-voltage V_G allows to shift the eigenenergies of the dot by $-eN_i V_G$ relative to the applied chemical potentials.

A similar rate equation approach has been used in [117, 118] within the charging model (3.1) where single electron states are populated or depleted while current flows. If the correlations among the quantum dot electrons are taken into account, ac-

cording to (3.2), it is crucial to keep the conservation of the total spin as a separate requirement for the transitions from **j** to **i** since the single electron states are mixed. In [8] has been assumed that the Clebsh-Gordan spin coupling coefficients determine the magnitude of

$$\Gamma_{\mathbf{ij}} \propto \begin{cases} \frac{S_{\mathbf{j}}+1}{2S_{\mathbf{j}}+1} & \text{for} \quad S_{\mathbf{i}} = S_{\mathbf{j}} + \frac{1}{2} \\ \frac{S_{\mathbf{j}}}{2S_{\mathbf{j}}+1} & \text{for} \quad S_{\mathbf{i}} = S_{\mathbf{j}} - \frac{1}{2} \\ 0 & \text{otherwise} \end{cases} , \tag{3.15}$$

where the dot spin changes from $S_{\mathbf{j}}$ to $S_{\mathbf{i}}$. In the presence of a magnetic field the spin states split into $(2S+1)$ Zeeman–levels and transitions are allowed only between adjacent z-components [181].

The selection rules (3.15) can cause the spin blockade. Two types of mechanisms are explained in [8, 183] and in [180, 188], respectively. The one is based on the high stability of the spin-polarized state because the electron escape transitions

$$(N, S = N/2) \longrightarrow (N-1, S' = (N-1)/2) \quad ,$$

which, in contrast to all other possible transitions, cannot increase the final spin but must reduce $S' = S - 1/2$. At sufficiently high applied voltages when energy allows occupation of the spin-polarized state its population is easy but its depopulation has a reduced probability. The high stationary population makes the other, better conducting states less populated which eventually causes the current drop. The overall behaviour of the differential conductance versus gate-voltage V_{G} and versus transport-voltage V is shown in Fig. 19 as a grey-scale plot. Along the $V = 0$ axis the linear conductance peaks [20] can be seen with Coulomb blockade regions in between. The lines parallel to the Coulomb blockade areas at finite V reflect the excitation spectrum of the quantum dot [181, 189]. The regions of negative differential conductances show up as bright lines. Very similar figures describe experiments [136, 190]. Figure 19 was obtained using the dot levels from Fig. 15 and solving (3.13) numerically.

The second mechanism for the occurrence of spin blockades requires at least two-dimensional quantum dots. It is based on high spin values of low energy states. Examples are the ground states for $N = 3$ or $N = 5$ electrons in a square-shaped hard wall confinement in two dimensions which have $S = 3/2$ (see Fig. 17). This influences even the linear transport behaviour since direct transitions to the ground states of the adjacent electron numbers $N = 2, 4$ are for spin reasons forbidden. The corresponding peak in the linear conductance should be "missing" at zero temperatures. Only finite temperature or transport-voltage may cause the conductance peak to recover if excited states with appropriate spin values become involved into transport. The corresponding observation in [191] can be explained along these lines [180]. "Slim" quantum dots should not exhibit missing linear conductance peaks.

The nonlinear transport has been investigated by solving numerically for the current, according to (3.14) and (3.13), for situations of high spin states close to the ground state energy. This can create negative differential conductances already at low transport voltages near the linear conductance peaks. Corresponding features were found experimentally in [136]. Also several aspects of the nonlinear transport properties in the presence of a magnetic field applied in the direction of the current,

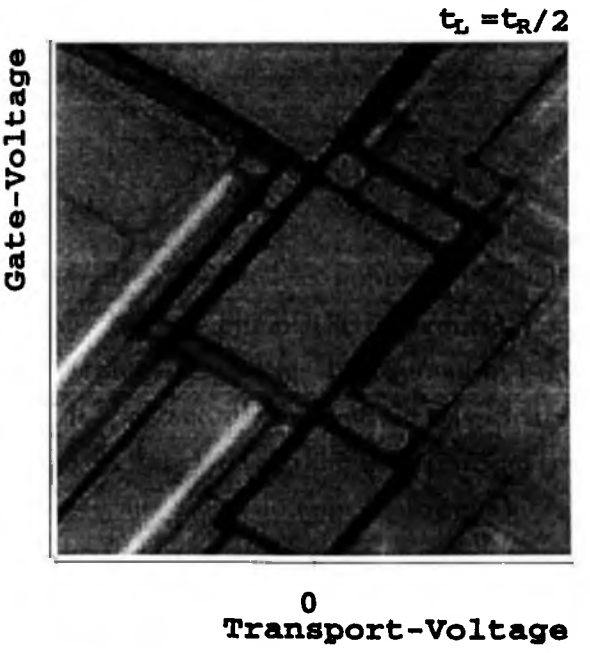

Fig. 19 Differential conductance versus gate- V_G and transport-voltage V. The zero-value inside the diamond-shaped Coulomb blockade regions corresponds to grey. Dark and bright parts indicate positive and negative differential conductances, respectively. For unequal couplings between dot and the leads $t_L = t_R/2$ bright regions are preferably found on one side of the transport voltage axis [8], in agreement with experiment [134].

causing only a Zeeman splitting of the dot levels, can be explained within the rate equation description provided the spin selection rules (3.15) are taken into account [181].

4 Summary and conclusions

Interesting physical consequences of the identity among strongly correlated, spin-carrying particles have been outlined. The low energy behaviour has been discussed in detail for two physical situations: rotational tunneling of molecules in solids and nonlinear transport properties of quantum dots. Both examples demonstrate strikingly how spin influences physical properties qualitatively.

In rotational tunneling molecules the identity of the protons or deuterons leads to very characteristic dissipative features. The tunneling line, observable e.g. by inelastic neutron scattering, is stable up to temperatures exceeding by far the tunneling energies. Two different types of environmental lattice vibrations can be distinguished experimentally by the negative or positive shifting behaviour of the tunneling line. The same dissipative 'phonon bath' influences decisively the temperature dependence of the extremely slow conversion transitions which provide thermal equilibration of the sample. The low temperature behaviour is completely determined by the coupling to 'breathing' type phonons which modulate the amplitude of the rotational potential. At temperatures somewhat above the tunneling energy librationally activated 'Orbach' processes start to dominate the conversion rate. They are determined by 'shaking' type phonons which modulate the phase of the rotational potential and lead to an Arrhenius type temperature dependence. Strong evidence exists that these different types of phonon couplings, investigated here for the triangular CH_3 rotors, play a similar

role in other rotational tunneling systems like CH_4 rotors. The consequences, summarized in Table 2, are in excellent agreement with experimental observations.

It has been demonstrated that isotopical substitution is a powerful probe for the microscopic surroundings of the rotors. Although the magnetic mechanisms for the conversion in deuterated and protonated systems differ considerably the dependence on temperatures T large compared to the tunneling energy Δ is found to be very similar and is determined by essentially the same dissipative environment. Then the major difference in the spin functions remains invisible. Phonons resonant with the respective librational transition energies are relevant, leading to the Arrhenius behaviour which is found in the experiments. Only for $T \lesssim \Delta$ or for almost freely rotating systems qualitative isotopical differences are predicted. The tunneling splitting in dimethyl-s-tetrazine, which has not been observed directly, could be extracted from the by two orders of magnitudes faster conversion in the deuterated species.

Also the low energy states and the transport properties of finite electron systems are qualitatively determined by spin. Contrary to weakly interacting situations the excitation spectra show multiplet structure, if the inter-particle repulsion decays slower than $\sim |x|^{-2}$ with the distance between the particles. This has been traced back to particle identity. The pocket state description, based on localized many particle states, enables a quantitative understanding of these spectra and yields the total spins of the individual levels by group theoretical means [193]. The results have been compared with exact numerical calculations. The spin explains the particularly striking negative differential conductances via selection rules. Two mechanisms for spin blockades involving high spin states at low energies have been mentioned.

The pocket state method can be applied to other strongly correlated few particle systems:

i) Orientationally coupled rotors have been considered [194] in order to extract information about the splitting behaviour of the tunneling line in the limit of strong coupling, that is inaccessible to the mean field approximation [195].

ii) The persistent current circulating in a ring of strongly interacting electrons in the presence of an Aharonov-Bohm flux turns out to be qualitatively influenced by the electron spin [33].

iii) Strong evidence appeared [32] that the pocket state approximation can serve as basis for a lattice description of initially *continuous* systems of strongly interacting electrons at low densities. This would allow to take advantage from rich experience to describe the low energy excitations in Hubbard models. Furthermore, theoretical studies about the very exciting problem of the interplay between interaction and disorder [196] could possibly be facilitated.

Several questions demand for further research. A closed theory to describe the dissipation in rotational tunneling systems, valid over the full range of temperatures and coupling strength's, is still lacking. The theory for symmetry species conversion needs to be completed by including the nuclear symmetry diffusion process which itself does not change the net amount of members of each symmetry species but which is essential for the macroscopic conversion of the whole sample in the presence of a low concentration of paramagnetic centers [103]. Corresponding experiments are proposed [197].

The experimental observation of total electron spins of ground and excited states in quantum dots of different electron numbers and shapes would be highly interesting, e.g. by sophisticated ESR-experiments [198]. The excitation energies in 'slim'

quantum dots should show ratios that are independent of the details of the $e^- - e^-$-interaction and of low electron densities $r_s^{-1} \ll a_B^{-1}$. Only the electron number should be relevant. In two–dimensional quantum dots it would be interesting to 'detect' the equilibrium position of electrons indirectly by comparing their excitation spectrum to a corresponding pocket state calculation.

One can speculate that many of the results obtained for the dissipation and the symmetry species conversion in rotational tunneling systems can be generalized accordingly to interacting electron systems. More than two slopes in the peak positions of the differential conductance versus an in-plane magnetic field would indicate spin changing transitions on time scales comparable with the mean time between electron passages through the contacts to a quantum dot. Inhomogeneous magnetic fields (imposed to the dot e.g. by trapped flux lines in a nearby piece of super-conductor) would act as strong paramagnetic impurity and should for instance show up in the suppression of negative differential conductances.

The author and the manuscript profited from the beneficial remarks of Alfred Hüller and the valuable advice of Bernhard Kramer which are gratefully acknowledged together with the joy about enlightening discussions with Gregor Diezemann, Kristian Jauregui, John Jefferson and Dietmar Weinmann.

References

[1] W. Pauli, Zeitschr. f. Physik **31** (1925) 765
[2] M. Hamermesh, Group Theory and its Applications to Physical Problems, Addison-Wesley, Massachusetts 62, new edition by Dover Publications, New York, 1989
[3] K.F. Bonhoeffer, P. Harteck, Ber. Berl. Akad. (1929) 103;
E. Cremer, M. Polanyi, Z. Phys. Chem. **B 21** (1933) 459
[4] W. Press, Single-Particle Rotations in Molecular Crystals, Springer Tracts in Modern Physics, Vol. 92, Springer, Berlin Heidelberg New York 1981
[5] H. Grabert, H. Wipf in: Advances in Solid State Physics, Vol. 30, (ed.), U. Rössler Vieweg, Braunschweig 1990
[6] I. F. Silvera, Rev. Mod. Phys. **52** (1980) 393
[7] A. Hüller, D.M. Kroll, J. Chem. Phys. **63** (1975) 4495
[8] D. Weinmann, W. Häusler, W. Pfaff, B. Kramer, U. Weiss, Europhys. Lett. **26** (1994) 467
[9] D. Pfannkuche, S.E. Ulloa, Phys. Rev. Lett. **74** (1995) 1194
[10] K. Jauregui, PhD thesis, Universität Hamburg, 1995
[11] K. Jauregui, W. Häusler, D. Weinmann, B. Kramer, Phys. Rev. **B 53** (1996) R1713
[12] D.V. Averin, K.K. Likharev, J. Low Temp. Phys. **62** (1986) 345
[13] H. Grabert, M. Devoret, Single Charge Tunneling, NATO ASI Series, Vol. 294, Plenum Press 1992, and refs. therein
[14] D.V. Averin, K.K. Likharev, in Quantum Effects in Small Disordered Systems, B.L. Altshuler, P.A. Lee, R.A. Webb (eds.), Elsevier, Amsterdam, 1991
[15] Special Issue on Single Charge Tunneling, H. Grabert (ed.), Z. Phys. B **85** (1991) 317–468
[16] T.A. Fulton, G.J. Dolan, Phys. Rev. Lett. **59** (1987) 109
[17] P. Delsing, K.K. Likharev, L.S. Kuzmin, T. Claeson, Phys. Rev. Lett. **63** (1989) 1861
[18] M.H. Devoret, D. Esteve, H. Grabert, G.-L. Ingold, H. Pothier, C. Urbina, Phys. Rev. Lett. **64** (1990) 1824
[19] H. Grabert, G.L. Ingold, M.H. Devoret, D. Esteve, H. Pothier, C. Urbina, Z. Phys. B **84** (1991) 143
[20] U. Meirav, M.A. Kastner, S.J. Wind, Phys. Rev. Lett. **65** (1990) 771
[21] L.P. Kouwenhoven, N.C. van der Vaart, A.T. Johnson, W. Kool, C.J.P.M. Harmanns, J.G. Williamson, A.A.M. Staring, C.T. Foxon, Z. Phys. B **85** (1991) 367;
L.P. Kouwenhoven, PhD thesis, Technical University of Delft, 1992
[22] L.J. Geerligs, C.J.P.M. Harmans, L.P. Kouwenhoven, The Physics of Few-Electron Nanostructures, North Holland, Physica B, Vol. 189, 1993
[23] Ch. Sikorski, U. Merkt, Phys. Rev. Lett. **62** (1989) 2164
[24] D. Pfannkuche, R.R. Gerhards, P.A. Maksym, V. Gudmundsson, in [22], p. 6

[25] D. Pfannkuche, V. Gudmundsson, P.A. Maksym, Phys. Rev. B **47** (1993) 2244
[26] D. Pfannkuche, R.R. Gerhards, Phys. Rev. B **44** (1991) 13132
[27] E.P. Wigner, Phys. Rev. **46** (1934) 1002
[28] K. Jauregui, W. Häusler, B. Kramer, Europhys. Lett. **24** (1993) 581
[29] R. Egger, H. Grabert, Phys. Rev. Lett. **75** (1995) 3505
[30] P.W. Anderson, Phys. Rev. **115** (1959) 2
[31] J. Hubbard, Proc. Royal Soc. London **A 276** (1963) 238
[32] J.J. Jefferson, W. Häusler, to appear in Phys. Rev. **B** (1996)
[33] W. Häusler, B. Kramer, in Quantum Dynamics of Submicron Structures, H.A. Cerdeira, B. Kramer, G. Schön (eds.), NATO ASI Series, Vol. 291, Kluwer, Dordrecht 1995;
W. Häusler, to appear in Physica **B** (1996)
[34] S. Chandrasekhar, Rev. Mod. Phys. **15** (1943) 1
[35] E. Kanai, Prog. Theor. Phys. **3** (1948) 440
[36] J.R. Ray, Am. J. Phys. **47** (1979) 626
[37] P. Ullersma, Physica **32** (1966) 27, 56, 74, 90
[38] F. Haake, R. Reinbold, Phys. Rev. A **32** (1985) 2462
[39] H. Grabert, P. Schramm, G.-L. Ingold, Phys. Rep. **168** (1988) 115
[40] A.O. Caldeira, A.J. Leggett, Phys. Rev. Lett. **46** (1981) 211;
A.O. Caldeira, A.J. Leggett, Annals of Physics **149** (1983) 374
[41] R.P. Feynman, Rev. Mod. Phys. **20** (1948) 367
[42] R.P. Feynman, A.R. Hibbs, Quantum Mechanics and Path Integrals, McGraw-Hill Inc., New York, 1965
[43] J. Adamowski, B. Gerlach, H. Leschke, J. Math. Phys. **23** (1982) 243
[44] R.P. Feynman, F.L. Vernon, Annals of Physics **24** (1963) 118
[45] U. Weiss, Quantum Dissipative Systems, World Scientific, Series in Modern Condensed Matter Physics, Singapore, 1993
[46] H. Grabert, U. Weiss, P. Hänggi, Phys. Rev. Lett. **52** (1984) 2193
[47] H. Grabert, U. Weiss, Phys. Rev. Lett. **53** (1984) 1787
[48] A.J. Leggett, S. Chakravarty, A.T. Dorsey, M.P.A. Fisher, A. Garg, W. Zwerger, Rev. Mod. Phys. **59** (1987) 1
[49] P. Hänggi, P. Talkner, M. Borkovec, Rev. Mod. Phys. **62** (1990) 251
[50] G.R. Fleming, P. Hänggi, Activated Barrier Crossing, World Scientific, Singapore, 1993
[51] L. van Hove, Phys. Rev. B **95** (1954) 249
[52] H.A. Kramers, Physica (Utrecht) **7** (1940) 284
[53] H. Grabert, S. Linkwitz, S. Dattagupta, U. Weiss, Europhys. Lett. **2** (1986) 631
[54] H. Wipf, K. Neumaier, Zeitschrift für Physikalische Chemie **164** (1989) 953
[55] R.F. Voss, R.A. Webb, Phys. Rev. Lett. **47** (1981) 265
[56] G. Schön, A. D. Zaikin, Physics Reports **198** (1990) 237
[57] H. Wipf, D. Steinbinder, K. Neumaier, P. Gutsmiedl, A. Magerl, A.-J. Dianoux, Europhys. Lett. **4** (1987) 1379
[58] M.W.G. Whittall, G.A. Gehring, J. Phys. C **20** (1987) 1619
[59] K.W.H. Stevens, J. Phys. C **16** (1983) 5765
[60] S. Clough, J. Phys. C **4** (1971) 2180
[61] S. Coleman, in International School of Subnuclear Physics, Majorana, 1977
[62] B. Felsager, Geometry, Particles and Fields, Odense University Press, Odense, Denmark, 1981
[63] L.S. Schulman, Techniques and Applications of Path Integration, John Wiley & Sons Interscience, New York 1981;
D.C. Khandekar, S.V. Lawande, Physics Reports **137** (1986) 115
[64] W. Häusler, Zur Temperaturabhängigkeit des Rotationstunnelns, PTB Bericht PG-3, ISBN 3-89429-002-1, Braunschweig 1990
[65] K.T. Hecht, D.M. Dennison, J. Chem. Phys. **26** (1957) 13
[66] A. Hüller, Z. Phys. B **36** (1980) 215
[67] S. Clough, B. Alefeld, J.-B. Suck, Phys. Rev. Lett. **41** (1978) 124;
S. Clough, A. Heidemann, J. Phys. C **12** (1979) 761;
S. Clough, A. Heidemann, M.N.J. Paley, J-B. Suck, J. Phys. C **13** (1980) 6599;
S. Clough, A. Heidemann, M.N.J. Paley, J. Phys. C **14** (1980) 1001;
M. Prager, K.-H. Duprée, W. Müller-Warmuth, Z. Phys. B **51** (1983) 309 and Z. Naturforsch. **39a** (1984) 1187;
A. Heidemann, S. Clough, P.J. McDonald, A.J. Horsewill, K. Neumaier, Z. Phys. B **58** (1958) 141
[68] M. Prager, J. Stanislawski, W. Häusler, J. Chem. Phys. **86** (1987) 2563
[69] A. Heidemann, M. Prager, M. Monkenbusch, Z. Phys. B **76** (1989) 25
[70] G. Diezemann, J. Phys.: Condens. Matter **4** (1992) 9153

[71] M. Prager, K.-H. Duprée, W. Müller-Warmuth, Z. Phys. B **51** (1983) 309
[72] A. Hüller, Phys. Rev. B **16** (1977) 1844;
A. Hüller, W. Press, Phys. Rev. B **24** (1981) 17
[73] P.W. Anderson, J. Phys. Soc. Jpn. **9** (1954) 316
[74] P.S. Allen, J. Phys. C **7** (1974) L22
[75] A.C. Hewson, J. Phys. C **15** (1984) 3841, 3855
[76] A. Würger, Z. Phys. B **76** (1989) 65
[77] A. Hüller, L. Baetz, Z. Phys. B **72** (1988) 47
[78] C. Deutsch, A. Hüller, Z. Phys. B **86** (1992) 411;
C. Deutsch, A. Hüller, Physica B **202** (1994) 320
[79] A. Hüller, Z. Phys. B **78** (1990) 125
[80] A. Vowe, J. Phys.: Condens. Matt. **5** (1993) 8531
[81] D. Braun, U. Weiss, Z. Phys. B **92** (1993) 507;
D. Braun, U. Weiss, Physica B **202** (1994) 264
[82] H. Grabert, U. Weiss, Z. Phys. B **56** (1984) 171
[83] M. Sassetti, U. Weiss, Phys. Rev. A **41** (1990) 5383
[84] M. Sassetti, M. Milch, U. Weiss, Phys. Rev. A **46** (1992) 4615
[85] U. Weiss, H. Grabert, P. Hänggi, P. Riseborough, Phys. Rev. B **35** (1987) 9535
[86] M. Prager, N. Wakabayashi, M. Monkenbusch, Z. Phys. B **94** (1994) 69
[87] M. Prager, C. Vettier, S. Mahling-Ennanoui, Z. Phys. B **75** (1989) 217
[88] A. Hüller, M. Prager, Solid State Comm. **29** (1979) 537
[89] K.J. Lushington, J.A. Morrison, Can. J. Phys. **55** (1977) 1580
H. Friedrich, K. Guckelsberger, R. Scherm, A. Hüller, J. Phys. C **14** (1981) L147
[90] S. Grieger, H. Friedrich, B. Asmussen, K. Guckelsberger, D. Nettling, W. Press, R. Scherm, Z. Phys. B **87** (1992) 203
[91] K. Guckelsberger, H. Friedrich, R. Scherm, Z. Phys. B **91** (1993) 209
[92] D. van der Putten, N.J. Trappeniers, Physica A **129** (1985) 302
[93] G. Diezemann, H. Sillescu, D. van der Putten, Z. Phys. B **83** (1991) 245
[94] A. Inaba, H. Chihara, J.A. Morrison, H. Blank, A. Heidemann, J. Tomkinson, J. Phys. Soc. Jpn. **59** (1990) 522
[95] A. Heidemann, K.J. Lushington, J.A. Morrison, K. Neumeier, W. Press, J. Chem. Phys. **81** (1984) 5799;
W. Press, A. Heidemann, H. Lauter, J. A. Morrison, K. Neumeier, Can. J. Phys. **66** (1988) 686
[96] G. Vandemaele, A. Buekenhoudt, L. van Gerven, J. Magn. Res. **89** (1990) 522
[97] C. von Borczyskowski, A. Oppenländer, H.P. Trommsdorff, J.-C. Vial, Phys. Rev. Lett. **65** (1990) 3277
[98] G. Gradl, K. Orth, J. Friedrich, Europhys. Lett. **19** (1992) 459
[99] C. Hartmann, M. Joyeux, H.P. Trommsdorff, J.-C. Vial, C. von Borczyskowski, J. Chem. Phys. **96** (1992) 6335;
K. Orth, P. Schellenberg, J. Friedrich, J. Chem. Phys. **99** (1993) 1
[100] K. Orth, P. Schellenberg, J. Friedrich, W. Häusler, J. Lumin. **56** (1993) 99
[101] K. Motizuki, T. Nagamiya, J. Phys. Soc. Jpn. **11** (1956) 93;
A.J. Berlinsky, W.N. Hardy, Phys. Rev. B **8** (1973) 5013
[102] A.J. Nijman, A.J. Berlinsky, Phys. Rev. Lett. **38** (1977) 408;
A. J. Nijman, A. J. Berlinsky, Can. J. Phys. **58** (1980) 1049
[103] G. Diezemann, W. Häusler, to appear in Physica B and unpublished
[104] W. Häusler, Z. Phys. B **81** (1990) 265
[105] A.A. Manenkov, R. Orbach, Spin-Lattice Relaxation in Ionic Solids, Harper & Row Publishers, New York Evanston London 1966
[106] A. Abragam, The Principles of Nuclear Magnetism, Clarendon Press, Oxford 1961
[107] C.P. Slichter, Principles of Magnetic Resonance, Springer, Berlin New York 1978
[108] L. van Gerven, G. Vandemaele, A. Buekenhoudt, 24th Ampere Congress on Magnetic Resonance and Related Phenomena, 1988;
A. Buekenhoudt, G. Vandemaele, L. van Gerven, Phys. Rev. B **41** (1990) 9038
[109] A. Würger, Z. Phys. B **81** (1990) 273
[110] G. Diezemann, W. Häusler, J. Phys.: Condens. Matter **5** (1993) 6121
[111] K. Orth, F. Rohlfing, J. Friedrich, Z. Phys. B **95** (1994) 493
[112] S. Grondey, M. Prager, W. Press, A. Heidemann, J. Chem. Phys. **85** (1986) 2204;
S. Grondey, M. Prager, W. Press, J. Chem. Phys. **86** (1987) 6465;
B. Asmussen, P. Gerlach, W. Press, M. Prager, H. Blank, J. Chem. Phys. **90** (1989) 1
[113] A. Heidemann, H. Friedrich, E. Günther, W. Häusler, Z. Phys. B **76** (1989) 335
[114] A. Heidemann, J. Eckert, L. Passel, W. Häusler, Z. Phys. B **66** (1987) 75

[115] J. Stanislawski, M. Prager, W. Häusler, Physica B **156** (1989) 356
[116] H.W. Spiess, NMR: Basic Principles and Progress, Vol. 15, P. Diehl, E. Fluck, R. Kosfeld (eds.), Spinger, Berlin 1978
[117] D.V. Averin, A.N. Korotkov, Sov. Phys. JETP **70** (1990) 937;
D.V. Averin, A.N. Korotkov, J. Low Temp. Phys. **80** (1990) 173;
A.N. Korotkov, D.V. Averin, K.K. Likharev, Physica B **165 & 166** (1990) 927
[118] D.V. Averin, A.N. Korotkov, K.K. Likharev, Phys. Rev. B **44** (1991) 6199
[119] C.W.J. Beenakker, Phys. Rev. B **44** (1991) 1646
[120] C. Bruder, H. Schoeller, Phys. Rev. Lett. **72** (1994) 1076
[121] G.-L. Ingold, Yu.V. Nazarov in [13], p. 21
[122] W. Zwerger, Z. Phys. B **93** (1994) 333
[123] H. Grabert, Physica B **194–196** (1994) 1011;
H. Grabert, Phys. Rev. B **50** (1994) 17364
[124] U. Meirav, M.A. Kastner, M. Heiblum, S.J. Wind, Phys. Rev. B **40** (1989) 5871
[125] M.A. Kastner, Rev. Mod. Phys. **64** (1992) 849
[126] M.A. Kastner, Physics Today (1993) 24, Jan.
[127] B. Meurer, D. Heitmann, K. Ploog, Phys. Rev. Lett. **68** (1992) 1371
[128] R.C. Ashoori, H.L. Stormer, J.S. Weiner, L.N. Pfeiffer, S.J. Pearton, K.W. Baldwin, K.W. West, Phys. Rev. Lett. **68** (1992) 3088;
R.C. Ashoori, H.L. Stormer, J.S. Weiner, L.N. Pfeiffer, S.J. Pearton, K.W. Baldwin, K.W. West, Physica B **189** (1993) 117;
R.C. Ashoori, H.L. Stormer, J.S. Weiner, L.N. Pfeiffer, K.W. Baldwin, K.W. West, Phys. Rev. Lett. **71** (1993) 613
[129] R.C. Ashoori, H.L. Stormer, J.S. Weiner, L.N. Pfeiffer, S.J. Pearton, K.W. Baldwin, K.W. West, Physica B **184** (1993) 378
[130] U. Merkt, Phys. Bl. **47** (1991) 509;
U. Merkt, Physica B **189** (1993) 165
[131] D. Heitmann, J.P. Kotthaus, in Physics Today, Vol. 56, June 1993
[132] A.T. Johnson, L.P. Kouwenhoven, W. de Jong, N.C. van der Vaart, C.J.P.M. Harmanns, C.T. Foxon, Phys. Rev. Lett. **69** (1992) 1592
[133] J. Weis, R.J. Haug, K. v. Klitzing, K. Ploog, Phys. Rev. B **46** (1992) 12837
[134] N.C. van der Vaart, A.T. Johnson, L.P. Kouwenhoven, D.J. Maas, W. de Jong, M.P. de Ruyter van Steveninck, A. van der Enden, C.J.P.M. Harmanns, Physica B **189** (1993) 99
[135] E.B. Foxman, P.L. McEuen, U. Meirav, N.S. Wingreen, Y. Meir, P.A. Belk, N.R. Belk, M.A. Kastner, S.J. Wind, Phys. Rev. B **47** (1993) 10020
[136] J. Weis, R.J. Haug, K. v. Klitzing, K. Ploog, Phys. Rev. Lett. **71** (1993) 4019
[137] P.L. McEuen, N.S. Wingreen, E.B. Foxman, J. Kinaret, U. Meirav, M.A. Kastner, Y. Meir, S.J. Wind, Physica B **189** (1993) 70
[138] Y. Meir, N.S. Wingreen, Phys. Rev. Lett. **68** (1992) 2512
[139] P.A. Lee, Physica B **189** (1993) 1
[140] Y. Meir, N.S. Wingreen, P.A. Lee, Phys. Rev. Lett. **70** (1993) 2601
[141] T. Inoshita, A. Shimizu, Y. Kuramoto, H. Sakaki, Phys. Rev. B **48** (1993) 14725
[142] K.A. Matveev, Phys. Rev. B **51** (1995) 1743
[143] M.H. Hettler, H. Schoeller, Phys. Rev. Lett. **74** (1995) 4907
[144] H. Schoeller, G. Schön, Phys. Rev. B **50** (1994) 18436
[145] T. Heinzel, S. Manus, D.A. Wharam, J.P. Kotthaus, G. Böhm, W. Klein, G. Tränkle, G. Weimann, Europhys. Lett. **26** (1994) 689
[146] G. Meissner, H. Namaizawa, M. Voss, Phys. Rev. B **13** (1976) 1370
[147] I.M. Tsidil'kovskiĭ, Sov. Phys. Usp. **30** (1987) 676
[148] D.M. Ceperly, B. J. Adler, Phys. Rev. Lett. **45** (1980) 566
[149] B. Lorenz, Phys. Stat. Sol. (b) **112** (1982) K47
[150] C.C. Grimes, G. Adams, Phys. Rev. Lett. **42** (1979) 795
[151] P.M. Platzman, H. Fukuyama, Phys. Rev. B **10** (1974) 3150
[152] A.V. Chaplik, Sov. Phys. JETP **35** (1972) 395
[153] T. Ando, A. B. Fowler, F. Stern, Rev. Mod. Phys. **54** (1982) 437
[154] H.J. Schulz, Phys. Rev. Lett. **71** (1993) 1864
[155] D. Pines, P. Nozières, The Theory of Quantum Liquids, Addison-Wesley Publishing Company, Redwood, California 1966, Vol. I+II, new edition, 1984
[156] J. Sólyom, Advances in Physics **28** (1979) 201;
V.J. Emery, in Highly Conducting One-Dimensional Solids, J.T. Devreese, R.P. Evrard, V.E. van Doren (eds.), Plenum Press, New York, London, 1979;
F.D.M. Haldane, J. Phys. C **14** (1981) 2585;

H.J. Schulz, in Correlated Electron Systems, V.J. Emery (ed.), World Scientific, Singapore, 1993, p. 199, see also [166];
B.G. Levi, Physics Today **47** (1994) 21
[157] B. Sutherland, J. Math. Phys. **12** (1971) 246;
B. Sutherland, Phys. Rev. A **4** (1971) 2019
[158] D.V. Averin, Yu.V. Nazarov, Phys. Rev. B **47** (1993) 9944;
D.V. Averin, Yu.V. Nazarov, Physica B **189** (1993) 241
[159] P.A. Maksym, T. Chakraborty, Phys. Rev. Lett. **65** (1990) 108
[160] U. Merkt, J. Huser, M. Wagner, Phys. Rev. B **43** (1991) 7320
[161] P. Hawrylak, D. Pfannkuche, Phys. Rev. Lett. **70** (1993) 485
[162] F. Bolton, Phys. Rev. Lett. **73** (1994) 158
[163] K. Jauregui, unpublished, shown here with kind permisson, from Ref. [10]
[164] G.W. Bryant, Phys. Rev. Lett. **59** (1987) 1140
[165] D.C. Mattis, Physics **1** (1964) 183
[166] G.D. Mahan, Many-Particle Physics, Plenum Press, New York London 1990
[167] E. Lieb, D. Mattis, Physical Review **125** (1962) 164
[168] W. Häusler, B. Kramer, Phys. Rev. B **47** (1993) 16353
[169] W. Häusler, B. Kramer, in Quantum Effect Physics, Electronics and Applications, K. Ismail, T. Ikoma, H.I. Smith (eds.), IOP Publishing Ltd., Institute of Physics Conference Series Vol. 127, Bristol, Philadelphia 1992
[170] W. Häusler, B. Kramer, J. Mašek, Z. Phys. B **85** (1991) 435
[171] L. Belkhir, Phys. Rev. B **50** (1994) 8885
[172] P.A. Maksym, Physica B **184** (1993) 385
[173] V.M. Bedanov, F.M. Peeters, Phys. Rev. B **49** (1994) 2667
[174] W. Häusler in: Advances in Solid State Physics, Vol. 34, R. Helbing (ed.), Vieweg, Braunschweig 1994;
W. Häusler, Z. Phys. **B99** (1996) 551
[175] E.P. Wigner, J.J. Griffin, Group Theory and its Applications to the Quantum Mechanics of Atomic Spectra, Academic Press, New York 1959
[176] A.D. Boardman, D.E. O'Connor, P.A. Young, Symmetry and its Applications in Sciences, McGraw-Hill Book Company, London, New York 1973
[177] D.E. Rutherford, Substitutional Analysis, The Edinburgh University Press, London, 1948
[178] K. Moulopoulos, N. W. Ashcroft, Phys. Rev. Lett. **69** (1992) 2555
[179] J.J. Palacios, L. Martin-Moreno, C. Tejedor, Europhys. Lett. **23** (1193) 495;
J.J. Palacios, PhD thesis, Universidad Autónoma de Madrid, 1993;
J.J. Palacios, L. Martin-Moreno, C. Tejedor, Surf. Sci. **305** (1994) 541
[180] D. Weinmann, W. Häusler, B. Kramer, Phys. Rev. Lett. **74** (1995) 984
[181] D. Weinmann, PhD thesis, Universität Hamburg, 1994
[182] W. Häusler, K. Jauregui, D. Weinmann, T. Brandes, B. Kramer, Physica B **194** (1994) 1325
[183] W. Pfaff, D. Weinmann, W. Häusler, B. Kramer, U. Weiss, Z. Phys. B **96** (1994) 201
[184] D. Averin, G. Schön, in Quantum Coherence in Mesoscopic Systems, Vol. 254, B. Kramer (ed.), NATO ASI Series, Plenum Press, 1991
[185] C. Bruder, R. Fazio, H. Schoeller, to appear in Phys. Rev. Lett. (1996)
[186] A. Yacoby, M. Heiblum, D. Mahalu, H. Shtrikman, Phys. Rev. Lett. **74** (1995) 4047
[187] N.C. van der Vaart, S.F. Godijn, Y.V. Nazarov, C.J.P.M. Harmans, J.E. Mooij, L.W. Molenkamp, C.T. Foxon, Phys. Rev. Lett. **74** (1995) 4047
[188] D. Weinmann, W. Häusler, K. Jauregui, B. Kramer, in Quantum Dynamics of Submicron Structures, Vol. 291, H. A. Cerdeira, B. Kramer, G. Schön (eds.), NATO ASI Series, Kluwer, Dordrecht, 1995.
[189] J. Weis, PhD thesis, University of Stuttgart, 1994
[190] J. Weis, R.J. Haug, K. v. Klitzing, K. Ploog, Semicond. Sci. Technol. **9** (1994) 1890
[191] J.T. Nicholls, J.E.F. Frost, M. Pepper, D.A. Ritchie, M.P. Grimshaw, G.A. Jones, Phys. Rev. B **48** (1993) 8866
[192] J. Weis, R.J. Haug, K. von Klitzing, K. Ploog, Physica B **189** (1993) 111
[193] R. W. Haase, N. F. Johnson, Phys. Rev. B **48** (1993) 1583
[194] W. Häusler, J. Phys.: Condens. Matter **4** (1992) 2577
[195] M. Timann, G. Voll, W. Häusler, J. Chem. Phys. **100** (1994) 8307
[196] D.L. Shepelyansky, Phys. Rev. Lett. **73** (1994) 2607;
D. Weinmann, A. Müller-Groeling, J.-L. Pichard, K. Frahm, Phys. Rev. Lett. **75** (1995) 1598
[197] H. Friedrich, private communication
[198] R.N. Ghosh, R.H. Silsbee, Phys. Rev. B **46** (1992) 12508